

OmniEarth-Bench: Towards Holistic Evaluation of Earth’s Six Spheres and Cross-Spheres Interactions with Multimodal Observational Earth Data

Fengxiang Wang^{1,2}, Mingshuo Chen³, Xuming He^{2,4}, Yi-Fan Zhang⁹, Yueying Li¹,
 Feng Liu^{2,5}, Zijie Guo⁶, Zhenghao Hu⁷, Jiong Wang^{2,6}, Jingyi Xu^{2,6}, Zhangrui Li^{2,8},
 Junchao Gong², Di Wang¹⁰, Fenghua Ling², Ben Fei², Weijia Li⁷, Long Lan¹, Wenjing Yang^{1*},
 Jing Zhang¹⁰, Wenlong Zhang^{2*}, Lei Bai²

¹ National University of Defense Technology, China

² Shanghai Artificial Intelligence Laboratory, China

³ Beijing University of Posts and Telecommunications, China

⁴ Zhejiang University, China ⁵ Shanghai Jiao Tong University, China ⁶ Fudan University, China

⁷ Sun Yat-sen University, China ⁸ Nanjing University, China

⁹ University of Science and Technology of China ¹⁰ Wuhan University, China

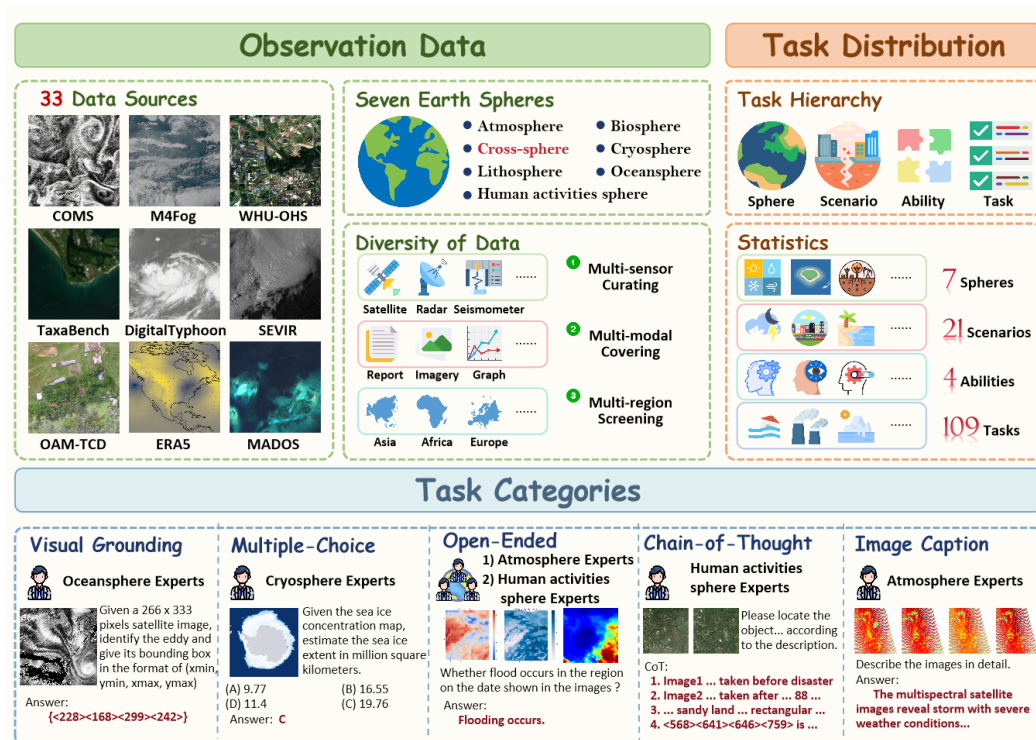


Figure 1: **Overview of OmniEarth-Bench.** Our benchmark spans six Earth science spheres and cross-sphere, encompassing 109 expert-curated tasks derived from 33 data sources. This involved the efforts of 20 experts and 45 crowd-sourcing annotators contributing to the annotations.

Abstract

Existing benchmarks for multimodal learning in Earth science offer limited, siloed coverage of Earth’s spheres and their cross-sphere interactions, typically restricting evaluation to the human-activity sphere or atmosphere and to at most 16 tasks.

*Corresponding authors

Holistically evaluating MLLMs on observational data across all Earth spheres faces three limitations: *multi-source heterogeneous data*, *unlocking scientific formulation*, and *cross-sphere reasoning*. Therefore, we introduce **OmniEarth-Bench**, the first multimodal benchmark that systematically spans all six spheres: atmosphere, lithosphere, oceansphere, cryosphere, biosphere, and human-activity sphere, and cross-sphere. Built with a scalable, modular pipeline that ingests 33 native Earth-observation sources and expert-in-the-loop curation, OmniEarth-Bench produces 29,855 standardized, expert-curated annotations. All annotations are organized into a four-level hierarchy (Sphere, Scenario, Ability, Task), encompassing 109 expert-curated evaluation tasks. Experiments on 9 state-of-the-art MLLMs reveal that even the most advanced models struggle with our benchmarks, where none of them reach 35% accuracy, revealing systematic gaps in Earth-system cognitive ability. The dataset and evaluation code were released at [OmniEarth-Bench](#).

1 Introduction

Earth scientists study critical environmental and societal problems by modeling Earth’s interconnected subsystems [6], such as the atmosphere, lithosphere, hydrosphere, cryosphere, biosphere, and human-activity sphere [76], which together determine planetary behavior and risks. Cross-sphere couplings underpin many high-impact discoveries and applications: for example, accurate flood prediction depends on atmospheric precipitation, biospheric soil moisture, and lithospheric runoff [85]. Earth Observational (EO) data from satellites and in-situ networks have expanded dramatically, creating an opportunity to use data-driven methods to reveal process couplings and improve monitoring, forecasting, and decision support in domains such as disaster response, ecosystem management, and climate science [64, 87, 53, 101].

Recently, multimodal large language models (MLLMs) and their benchmarks have advanced core capabilities, including visual perception, long-context modeling, and chain-of-thought (CoT) reasoning [50, 80, 19, 42, 66, 98, 33]. In remote sensing, a growing array of multimodal benchmarks has been introduced to tackle large-scale [86, 51], multispectral [97, 72], and other applications [102, 45]. Atmospheric science is now following suit, deploying multimodal models for severe weather events [52], meteorological heatmaps [9], and climate event forecasting [43]. Given that the Earth system comprises six major spheres and their intricate couplings, we face an overarching challenge: **how can we holistically evaluate MLLMs’ cognitive ability under a unified benchmark for observation data across all spheres?** We identify three key attributes of Earth science that give rise to this challenge:

(1) **Multi-source heterogeneous data:** EO data are multi-source and heterogeneous (e.g., multi-spectral satellite imagery, seismic signals, weather reanalysis, microwave sea-ice concentration), demanding careful spatiotemporal co-registration, quality control, and variable/units harmonization across sensors and scales to yield credible labels and supervision for cross-sphere tasks. *Observation Data* in Fig 1 show that heterogeneous EO data cover six earth spheres and cross-sphere.

(2) **Unlocking scientific formulation:** Across Earth science, many tasks demand fine-grained scientific reasoning—for example, multifaceted diagnosis of the El Niño–Southern Oscillation (ENSO) [26] and carbon-flux estimation [18] that quantifies exchange rates between the biosphere and the atmosphere. Creating authoritative evaluation dimensions requires domain experts to define scientifically meaningful, sphere-specific tasks and to assess each dimension’s suitability as a target for MLLM evaluation. *Task Distribution* and *Task Categories* in Fig. 1 show that each sphere requires coordinated, discipline-specific experts to unlock scientific formulation.

(3) **Cross-sphere reasoning:** Many Earth processes are intrinsically cross-sphere (e.g., precipitation-soil-runoff, ocean–atmosphere ex-

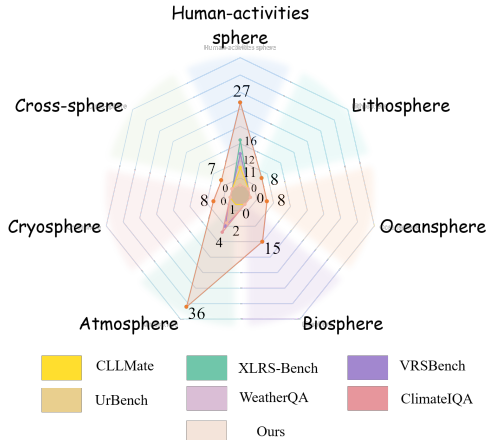


Figure 2: **Comparison of Different Benchmarks.** Our OmniEarth-Bench shows the broadest coverage, with dedicated cross-sphere dimensions.

Table 1: **Comparison between existing vision-language benchmarks and our benchmark.** ✘ represents semi-automated, *i.e.*, machine generation followed by human verification.

Dataset	Spheres	Cross-Sphere	Observation Data	Data Source Volume	Task		
					Volume	Dimensions Volume	Expert Annotation
ScienceQA [66]	✘	✘	✘	-	21,000	127	✘
Seed-Bench [42]	✘	✘	✘	-	19,242	12	✘
MME [19]	✘	✘	✘	-	2,374	14	✔
MMBench [50]	✘	✘	✘	-	3,217	20	✔
MME-Realworld [98]	✘	✘	✘	-	29,429	43	✔
ZeroBench [65]	✘	✘	✘	-	100	✘	✘
MME-CoT [33]	✘	✘	✘	-	1,130	✘	✘
VRSBench [46]	human-activity sphere	✘	✔	2	175,703	12	✘
XLRS-Bench [86]	Human-activity sphere	✘	✔	6	45,008	16	✔
RSIEval [29]	Human-activity sphere	✘	✔	1	933	1	✘
UrBench [102]	Human-activity sphere	✘	✔	6	11,600	11	✘
WeatherQA [52]	Atmosphere	✘	✔	1	8,000	2	✘
ClimateQA [43]	Atmosphere	✘	✔	2	254,040	4	✘
CLLMate [43]	Atmosphere	✘	✔	2	7,747	1	✘
OmniEarth-Bench	6 Spheres	✔	✔	33	29,855	109	✔

change), models and evaluations must capture interactions rather than isolated patterns. This requires domain experts to formalize the interaction pathway and identify a scientific definition set across spheres and to translate these agreements into evaluation criteria that faithfully reflect inter-sphere dynamics. A cross-sphere example in the *Task Categories* of Fig. 1 shows that cross-sphere tasks require coordinated expertise from experts across different spheres.

In this paper, we introduce **OmniEarth-Bench**, a systematic benchmark to evaluate the cognitive ability of MLLMs across all six Earth science spheres and their couplings. To ensure scientific validity, we engaged 2-5 domain experts per sphere to define evaluation dimensions and select or curate relevant observational datasets (e.g., MODIS and other satellite/in-situ sources). The annotation team (20 experts plus 45 crowd annotators) produced and quality-checked 29,855 expert-curated annotations organized into a four-level hierarchy (Sphere, Scenario, Ability, Task). The final benchmark contains 109 L-4 Tasks across seven thematic spheres (the six spheres plus an explicit cross-sphere). As shown in Fig. 2 and summarized in Tab. 1, OmniEarth-Bench substantially expands both the breadth and scientific coherence of EO evaluation compared with prior work. Our evaluations across nine state-of-the-art MLLMs reveal large and systematic failure modes (none exceed 35% overall accuracy), demonstrating the pressing need for Earth-system modeling and specialized reasoning mechanisms.

The key contributions are:

- **A unified Earth-observation processing pipeline.** We build a scalable, modular pipeline that ingests 33 native Earth-science data sources and, via expert-in-the-loop curation, produces 29,855 standardized, expert-curated annotations by 20 domain experts and 45 annotators to constitute the OmniEarth-Bench evaluation set.
- **A four-level, sphere-complete evaluation framework.** We provide the first benchmark that systematically covers all six Earth spheres and explicit cross-sphere scenarios, organized into a four-level hierarchy with 109 L-4 sub-dimensions to measure breadth and real-world relevance beyond prior, siloed EO benchmarks.
- **Comprehensive evaluations.** Comprehensive evaluations on nine state-of-the-art MLLMs reveal that even the most advanced models struggle with our benchmarks. Especially, in some cross-sphere tasks, the performance of leading models like GPT-4o drops to 0.0%.

2 Related Work

Earth Multimodal Benchmark. Recent advancements in large multimodal models (MLLMs) have accelerated progress in Earth sciences [39, 58], leading to the development of several evaluation benchmarks [46, 86, 52, 9]. Current benchmarks primarily target the human-activity sphere and atmosphere. In the human-activity sphere, remote sensing-based benchmarks include RSIEval [29], VRSBench [46], XLRS-Bench [86], and so on. Atmospheric benchmarks include WeatherQA [52], ClimateIQA [9] and CLLMate [43]. **However, these benchmarks exhibit notable limitations:** 1)

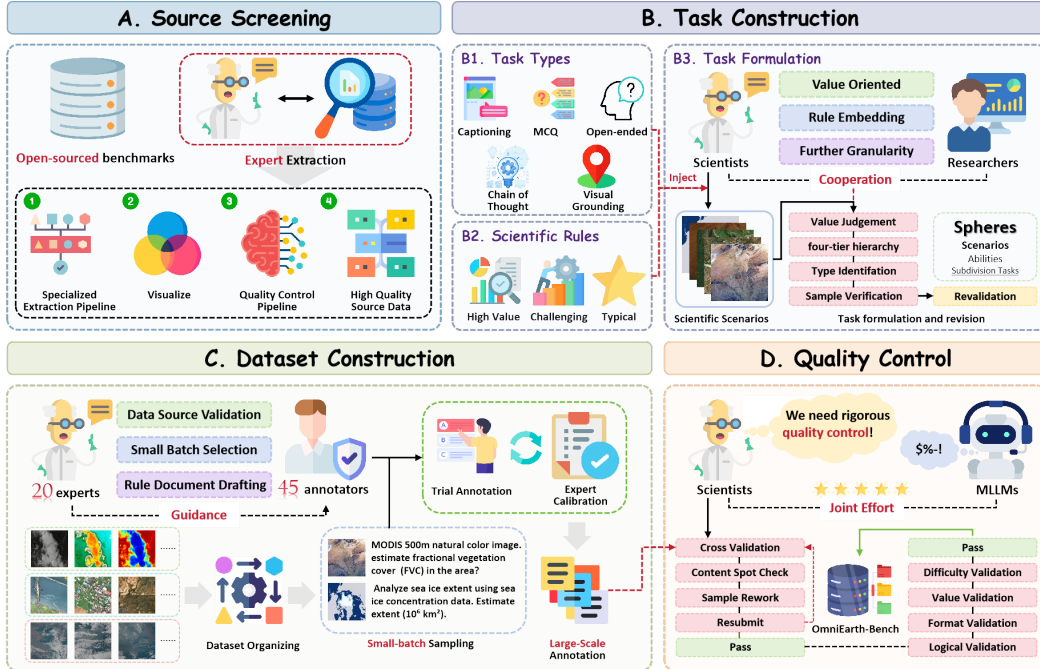


Figure 3: **Pipeline of OmniEarth-Bench.** Our pipeline comprises 4 stages: Source Screening, Task Construction, Dataset Construction, and Quality Control, all led by experts. The first two stages are exclusively conducted by experts, while crowd-sourcing annotators assist in the latter two stages.

They typically address isolated spheres, neglecting cross-sphere interactions essential to real-world Earth science challenges. 2) They offer limited evaluation dimensions, for example, atmospheric benchmarks assessing fewer than four question types.

General Multimodal Benchmark. Large-scale vision-language models (VLMs) have shown great promise in multimodal tasks such as scene understanding and visual sentiment analysis, prompting the development of diverse benchmarks to quantitatively assess their capabilities. However, earlier benchmarks mostly targeted specific domains with limited evaluation tasks (*e.g.*, visual grounding [75, 93] or visual question answering (VQA) [32, 54, 22, 25, 70]). Recent efforts aim for more comprehensive assessments: MME [19], MMBench [50], Seed-Bench [42], MMT-Bench [90], MME-Realworld [98], HLE [62] and MMMU-Pro [92]. Multimodal chain-of-thought (CoT) benchmarks were also developed, such as MME-CoT [33] and ZeroBench [65]. Despite these advancements, **two critical limitations remain:** 1) Earth sciences have been largely neglected, with only SuperGPQA featuring a minimal number (only 100 annotations) of geophysics-related textual questions. 2) Existing benchmarks overlook the importance of observational data, a distinctive strength of Earth sciences (*e.g.*, climate data grids, seismic signals).

3 OmniEarth-Bench

3.1 Pipeline of Benchmark

Source Screening. Our Benchmark comprises not only publicly available open-source datasets but also a significant portion of data manually extracted by experts from satellite imagery and raw observational sources. For example, Vegetation Monitoring uses satellite imagery from MODIS and expert-curated data from the Global Land Surface Satellite (GLASS), including Leaf Area Index, Fractional Vegetation Cover, and Peak Vegetation Coverage Area. Moreover, for the Eddy data in oceansphere, the chlorophyll (CHL) data used in this study were obtained by applying the OCI empirical algorithm to Level-2 data acquired by the Geostationary Ocean Color Imager I (GOCI) aboard the Oceanography and Meteorology Satellite (COMS). After careful selection and integration, we compiled a dataset originating from 33 distinct data sources spanning all Earth spheres. It is crucial to clarify that *33 data sources* refers to the raw data origins, not 33 different input modalities (*e.g.*, individual spectral bands or 1D signals). To ensure fair evaluation, domain experts processed all

Table 2: **Data source of different spheres**, including open-source datasets, satellite websites, and other observation data sources. We only exhibit the L1 and L2 dimensions. Processing pipeline for each data source is shown in the Appendix A.3.

L1 dimenons	L2 deminesons	Data Source	Annotations Volume
Cross-sphere	Global Flood Forecasting	GFF [85]	873
	Bird Species Prediction	SatBird [78]	2,253
	Carbon Flux Monitoring	CarbonSense [18]	330
Human-activity sphere	Urban Construction	UBCV1 [31]	3,161
	Land Use	WHU-OHS [44]	2,990
	Surface Disaster Assessment	XView [24]	3,851
Biosphere	Species Distribution Prediction	TreeSatAI [4]	2,819
	Vegetation Monitoring	OAM-TCD [82]	900
	Environmental Pollution Monitoring	GLASS [47]	246
	Human Footprint Assessment	ROSID [59]	600
	Crop Growth Monitoring	HFP [67]	1,656
Atmosphere	SEVIR Weather	MOPAD [99]	893
	Typhoon Events	SEVIR [81]	5,082
	Short-term meteorological events	DigitalTyphoon [37]	140
	Medium-term meteorological events	ERA5 [28]	160
	Seasonal meteorological events	ERA5 [28]	60
	Interannual climate change	ERA5 [28]	60
Lithosphere	Earthquake monitoring and prediction	STRAD [57]	1,500
	Geological exploration imaging	TGS-Salt [34]	631
Oceansphere	Marine Debris and Oil Pollution	MADOS [36]	221
	Marine Extreme Events	ERASSTv5 [30]	583
	Marine Phenomenon Detection	COMS [89],	570
Cryosphere	Sea ice forecast	G02202 (SIC) [56]	200
	Glacier analysis	PIOMAS [69]	30
			CryoSat-2 [27]
		IceBridge [74]	

data into MLLM-compatible formats, applying specific strategies tailored to the data characteristics of each sphere. This process prioritized the native data structure; for instance, multi-spectral data was converted into multiple single-channel grayscale images to avoid a dependency on potentially misleading RGB visualizations. Tab.2 is a summary of the data sources used for each Earth sphere, with detailed data organization and construction procedures presented in the Appendix A.3.

Task Construction. As shown in Fig.3, OmniEarth-Bench defines tasks across four hierarchical levels (L1-L4): L1 covers the seven domains based on established geophysical spheres: atmosphere, lithosphere, oceansphere, cryosphere, biosphere, human-activity sphere, and cross-sphere. L2 includes expert-approved, representative scenarios within each sphere, selected based on their scientific and practical value (e.g., earthquake prediction). Tab.2 illustrates representative scenarios covered by the L1 and L2 levels. Detailed descriptions of the L3 and L4 dimensions for each sphere are provided in the Appendix A.5 and Appendix A.6. L3 comprises four core abilities: Perception, General Reasoning, Scientific-Knowledge Reasoning, and CoT Reasoning. Perception and General Reasoning align with previous works such as MMBench [50] and XLRS-Bench [86], where Perception focuses on sensory inputs and Reasoning on inference. Scientific-Knowledge Reasoning addresses complex reasoning tasks requiring deep domain expertise in Earth sciences. CoT Reasoning evaluates the effectiveness of chain-of-thought processes within Earth science scenarios. L4 provides further granularity by subdividing tasks based on the L1-L3 dimensions. Achieving robust general intelligence in Earth sciences requires MLLMs to perform effectively across all hierarchical levels.

Benchmark Construction. For each of the six Earth spheres, this involved a dedicated team of 2-5 experts (Ph.D. holders or candidates) and 5—10 annotators (undergraduate and master’s students). (1) For each sphere, evaluation dimensions were collaboratively defined by domain experts and MLLM specialists, ensuring high practical value and complexity. Cross-sphere tasks involved experts from multiple domains. This approach addresses the limitations observed when crowd-sourcing annotators proposed overly simplistic tasks—for example, “Estimated Maximum Precipitation Level” in atmosphere, which GPT-4o solved with 97.7% accuracy. Expert-led design ensures meaningful evaluation. (2) Experts were also responsible for defining data sources. For complex tasks, crowd-

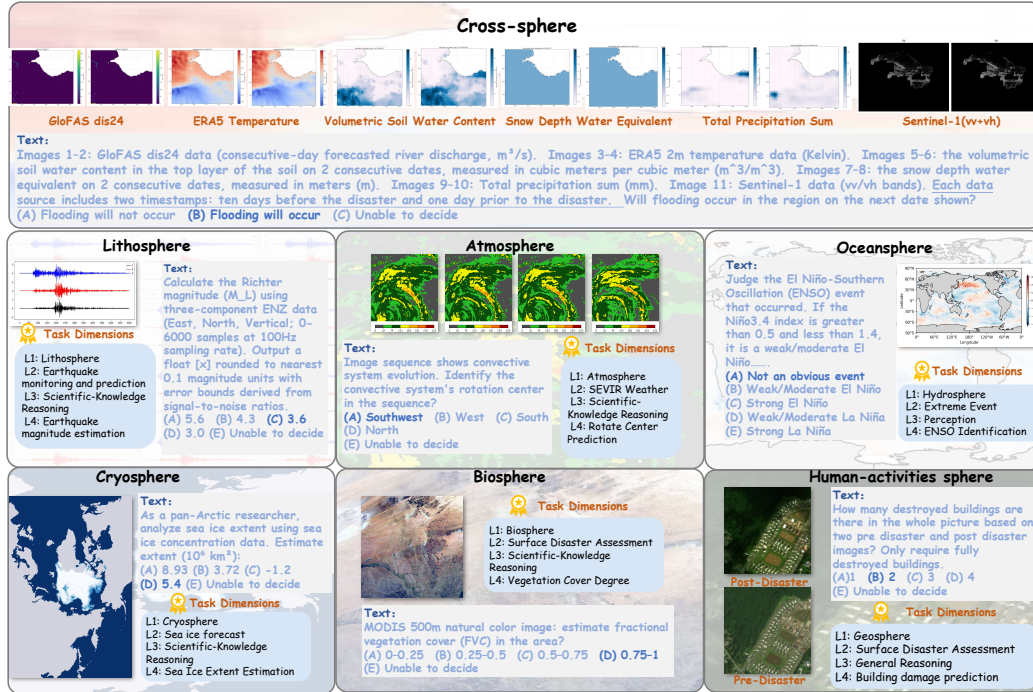


Figure 4: **Examples of OmniEarth-Bench.** OmniEarth-Bench comprises 109 unique L4 tasks, each with distinct questions, answers, and images.

sourcing annotators struggled with downloading and aligning data (e.g., MODIS and GLASS from NASA). Thus, experts curated and organized datasets, with annotators assisting.

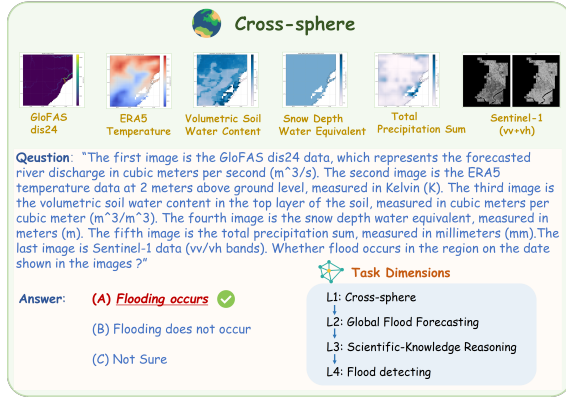
Quality Control. To ensure data integrity and task relevance, the quality control process involved two main steps. Cross-Validation: Annotator outputs were systematically compared against expert-provided annotation examples. Any discrepancies were flagged and reviewed by domain experts to ensure annotation correctness, especially for complex tasks involving multi-source data. Final Quality Assessment: specialists conducted thorough reviews to confirm that annotations adhered to expert standards and maintained consistency across all tasks and spheres. High-quality annotations were approved and incorporated into the dataset, while annotations that did not meet quality standards underwent iterative refinement through a feedback loop involving annotators and expert supervision. This cyclical process ensured continuous improvement and maintained reliability.

3.2 Task Dimensions

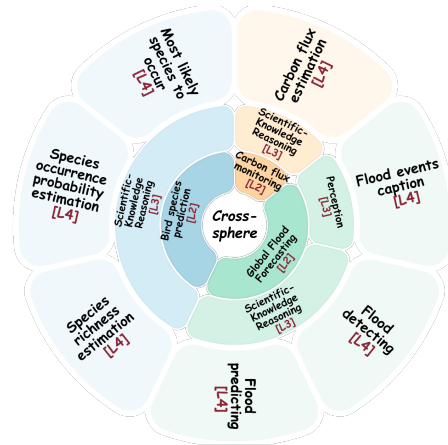
OmniEarth-Bench defines tasks across four hierarchical levels (L1-L4), comprising 7 L1 dimensions, 25 L2 dimensions, 5 L3 dimensions, and 109 expert-defined L4 subtasks with real-world applicability. One representative L4 subtask from each L1 sphere is illustrated in Fig 4. We offer cross-sphere as an example of the L1-L4 divisions, with details for other spheres given in the Appendix A.7.

Cross-sphere tasks in Earth science carry high practical and societal importance [15, 14]. As shown in Fig 5, we select three representative L2 scenarios from socially impactful applications, including *Global Flood Forecasting (L2)*, *Bird Species Prediction (L2)* and *Carbon Flux Monitoring (L2)*. Due to their reliance on expert knowledge and complex reasoning, all are categorized as Scientific-Knowledge Reasoning (L3). Despite the complexity of cross-sphere scenarios, we successfully collaborated with domain experts to construct **7 high-value subtasks (L4 dimensions)**. Further details on full tasks are available in the Appendix A.2. Overall, the L1-L4 divisions provide a coherent evaluation framework across Earth science spheres, with dimensions designed by domain experts to ensure high value.

3.3 Statistics and Analyses



(a) An example in Cross-sphere.



(b) Task hierarchy of cross-sphere (L1-L4 dimension).

Figure 5: **Details of Dimension in Cross-sphere.** Cross-sphere has 3 L-2 dimensions, 2 L-3 dimensions and 7 L-4 dimensions.

Overview Statistics. OmniEarth-Bench includes 109 expert-defined, high-value evaluation dimensions and 29,855 samples annotated by both experts and crowd-sourced contributors. As shown in Tab. 1, it offers clear advantages over existing benchmarks. Uniquely built on observational Earth science data—rather than exam-style datasets—OmniEarth-Bench spans all six spheres and cross-sphere scenarios. Consistency metrics are reported in Tab. 3, with additional details and dimension-specific indicators provided in the Appendix A.2.

Observational Data vs. Exam-questions Data. Unlike subject-based benchmarks like ScienceQA [66], which rely on exam questions or online learning problems followed by manual filtering, our approach takes a fundamentally different path. While such methods could theoretically span all six Earth spheres, they face two key limitations: (1) Benchmarks like ScienceQA focus on scientific inquiry rather than practical geoscience applications, limiting their real-world relevance. (2) Their evaluation dimensions are constrained by a bottom-up design: questions are derived from existing image-text pairs in papers, then filtered and categorized. In contrast, OmniEarth-Bench follows a top-down strategy: domain experts first define evaluation dimensions based on real-world geoscience challenges and data availability, then curate corresponding data. This ensures each task is both meaningful and grounded in practical utility.

4 Experiment

4.1 Experimental Setup.

The MLLMs evaluated on OmniEarth-Bench are grouped into two categories: (a) open-source VLMs, including Qwen2.5-VL [88], LLaVA-Onevision [41], InterVL3 [10] and InternLM-XComposer-2.5 [96]; (b) closed-source VLMs, such as GPT-4o [61], Gemini-2.0 [77] and Claude 3.7 Sonnet [3]. All models were evaluated using LMMS-Eval [95, 40]. Details of the evaluation are shown in Appendix A.4 and our code.

Table 3: **Main statistics of OmniEarth-Bench**

Statistic	Number
Total questions	29,855
- Cross-sphere	3,456
- Human-activity sphere	9,362
- Biosphere	6,221
- Atmosphere	6,395
- Lithosphere	2,131
- Oceansphere	1,374
- Cryosphere	230
Question Formats	
- Multiple-choice questions	27,082
- Open-ended questions	27,082
- Visual grounding questions	2,697
- CoT questions	610
- Images caption	76
MCQ	
- Single-image questions	24,108
- Multi-image questions	5,671
- Maximum question length	213
- Average question length	48.2
CoT	
- Total key step annotation	3,473
- Average key step annotation	5.8
- Average key step length	14.8
- Maximum question length	101
- Average question length	50.2
Caption	
- Average word length	133.5
- Average sentence length	4.5

Table 4: **Experimental results on each sphere of VQA tasks, with models ranked by average performance.** 'Avg' represents the average accuracy across sub-tasks. 'Experts' means evaluation results of 100 examples in each sphere by experts. We mark the highest score of each metric in red, and the second highest underlined. Here, Cross., Atmo., Litho., Ocean., Cryo., Bio., and Human. stand for Cross-sphere, Atmosphere, Lithosphere, Oceansphere, Cryosphere, Biosphere, and Human-activity sphere.

Method	Spheres (L1 dimensions)							Avg.
	Cross.	Atmo.	Litho.	Ocean.	Cryo.	Bio.	Human.	
Experts	90	96	91	95	93	97	95	93.4
Multiple choice question								
<i>Open-source MLLMs</i>								
Claude-3.7-Sonnet [3]	<u>30.68</u>	24.72	28.15	<u>23.12</u>	54.46	31.21	11.18	29.07
Gemini-2.0 [77]	16.93	20.83	38.94	16.94	<u>58.52</u>	20.83	23.74	28.10
GPT-4o [61]	0.04	9.64	12.80	13.35	37.48	1.97	2.76	11.15
<i>Open-source MLLMs</i>								
InternVL3-72B [104]	19.19	33.98	23.39	20.22	74.56	<u>31.99</u>	<u>29.46</u>	33.26
InternVL3-7B [104]	42.85	30.10	<u>37.47</u>	20.28	49.27	28.74	23.18	<u>33.13</u>
LLaVA-Onevision-7B [41]	19.26	<u>33.69</u>	28.72	24.54	46.40	37.31	30.62	31.51
InternLM-XComposer-2.5-7B [16]	19.78	17.45	28.88	21.06	40.04	30.67	24.76	26.09
Qwen2.5-VL-7B [5]	9.85	9.25	18.65	13.95	17.85	10.94	6.23	12.39
Qwen2.5-VL-72B [5]	3.92	4.82	22.43	16.27	5.88	14.91	8.63	10.98
Open-ended question								
<i>Closed-source MLLMs</i>								
Gemini-2.0 [77]	31.48	38.10	41.67	24.97	61.49	27.33	<u>31.85</u>	36.70
GPT-4o [61]	25.76	23.21	33.13	25.17	46.46	13.65	17.17	26.36
<i>Open-source MLLMs</i>								
InternVL3-72B [104]	<u>29.51</u>	39.14	27.51	32.45	<u>53.87</u>	38.29	34.67	<u>36.49</u>
Qwen2.5-VL-72B [5]	24.78	22.08	<u>38.62</u>	<u>31.17</u>	15.23	20.22	16.87	24.14

4.2 Main Results

All MLLMs exhibit suboptimal performance across all 7 spheres. As illustrated in Tab. 4 and Tab. 7, nearly all MLLMs achieve accuracy rates below 40%, significantly underperforming relative to their success on traditional perception or reasoning benchmarks [50, 55, 70]. Several factors likely contribute to this challenge. First, current multimodal large models are typically trained without domain-specific Earth science data, which impedes their ability to comprehend related queries. Second, many Earth science problems are inherently complex, particularly cross-domain prediction tasks that demand in-depth, specialized knowledge, which existing LLMs or MLLMs may not possess. Finally, OmniEarth-Bench provides high-resolution, intricate imagery, and the task of interpreting such complex visuals presents unique obstacles for MLLMs. This underscores the pressing need for specialized models or advanced post-training techniques to effectively address these challenges.

CoT Performance. Following the MME-CoT [33], we leverage two interpretable metrics to evaluate the CoT correctness: recall and precision. The two metrics respectively attend to the two aspects of the CoT correctness: informativeness and accuracy. As shown in Tab. 5, InternVL3 outperformed Qwen2.5-VL and LLaVA-OneVision with the highest F1 score. Larger open-source variants showed superior performance, underscoring the scalability of model size.

Table 5: **CoT performance on OmniEarth-Bench**

Models	LLaVA-OneVision-7B	Qwen2.5-VL-7B	InternVL3-8B	InternVL3-78B
Precision	89.83	92.72	94.02	94.74
Recall	23.41	29.12	34.47	35.5
F1	37.14	44.32	50.45	51.65

Table 6: **Images caption performance on OmniEarth-Bench**

Method	BLEU-1	BLEU-2	BLEU-3	BLEU-4	METEOR	ROUGE_L	CIDEr
<i>Closed-source MLLMs</i>							
Claude-3.7-Sonnet	5.45	2.46	1.04	0.36	5.54	6.13	1.34
GPT-4o	5.05	2.61	1.43	0.86	6.57	6.98	0.00
<i>Open-source MLLMs</i>							
Qwen2.5-VL-7B	3.59	1.39	0.63	0.30	4.06	3.77	0.44
Qwen2.5-VL-72B	5.22	2.21	0.95	0.41	5.99	6.15	0.00

Caption performance. As shown in Tab. 6, the closed-source models, particularly GPT-4o, demonstrated the strongest overall performance. However, the large open-source model Qwen2.5-VL-72B achieved highly competitive results, significantly narrowing the gap. The substantial performance leap from the 7B to the 72B version of Qwen2.5-VL strongly underscores the effective scalability of model size for improving caption generation capabilities.

Visual grounding performance. As shown in Tab.7, visual grounding on OmniEarth-Bench is low across spheres and IoU thresholds: only InternVL3-78B leads in Oceansphere (Acc@0.5=13.86), and human-activity sphere is hardest (peak 2.36), with general-purpose MLLMs near zero. The weakness stems from domain shift to earth observation data (large-scale variation, clutter, small/elongated targets) and insufficient multi-scale alignment, which inflate errors at higher IoU.

Table 7: Visual grounding performance on OmniEarth-Bench.

Spheres	Metrics	GPT-4o	Gemini-2.0	Claude-3.7-Sonnet	Qwen2.5-VL	LLaVA-OneVision	InternVL3 8B	InternVL3 78B
Human-activity sphere	Acc@0.5	0.02	0.03	0	0.59	0.2	0	2.36
	Acc@0.7	0	0	0	0	0	0	0.2
Lithosphere	Acc@0.5	0.08	0.13	0.02	5.3	0	8.94	4.3
	Acc@0.7	0	0.04	0	0.33	0	1.66	0.33
Oceansphere	Acc@0.5	0.12	0.34	0.2	1.81	1.51	6.63	13.86
	Acc@0.7	0.01	0.06	0.07	0	0	0.6	3.61

4.3 Further Analysis

MCQ-style vs. Open-ended evaluation. Results in Tab. 4 show that open-ended evaluation often yields higher scores, as models are free to respond in natural language without being constrained by pre-defined choices. This setting better reflects real-world usage, where models are expected to articulate answers directly. In contrast, MCQ-style evaluation offers a more standardized and objective framework. By providing fixed answer choices, it reduces ambiguity in scoring and ensures comparability across models. The inclusion of an “Unable to decide” option further mitigates the risk of models producing answers that appear reasonable but are logically inconsistent. As a result, while open-ended evaluation captures the flexibility of natural language reasoning, MCQ-style benchmarks remain valuable for delivering fair and rigorous assessments.

Time-sensitive task. The Earth’s seven spheres encompass numerous temporally correlated tasks. ENSO, a key climate mode influencing global weather extremes via teleconnections [79], has seen improved forecasts through domain-specific AI models [26, 23]. As shown in Fig. 6, prediction accuracy declines with longer lead times, echoing the limitations of specialized models. However, the performance of MLLMs still lags behind tailored models. Performance drops further for Indian Ocean Dipole (IOD) predictions, aligning with challenges faced by existing methods [49].

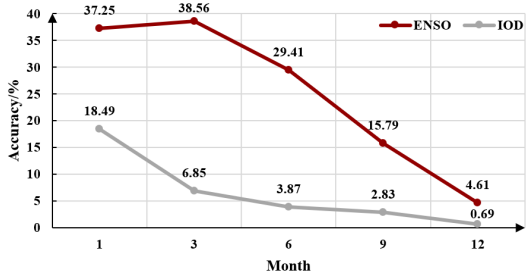


Figure 6: GPT-4o performance on ENSO and IOD prediction with different lead months (previous).

Limited Gains from Scaling Model Size on Earth-Science Tasks. In Table 4, we evaluate two sizes of the InterVL3 model and find that the 72B InterVL3 does not provide a significant advantage over the 7B model in our benchmarks, with performance even declining in some evaluation metrics. This contrasts with the substantial improvements observed in general-domain tasks. This performance bottleneck likely stems from the lack of Earth-science-specific knowledge, rather than a limitation in model capacity. Even large MLLMs struggle to reason about unfamiliar scientific concepts without targeted training on domain-specific data. These findings highlight the importance of prioritizing the integration of domain-specific knowledge in future Earth-science MLLM development, rather than merely increasing model size.

Impact of Model Safety on Results. In Tab. 4, we observe that Qwen2.5-VL and GPT-4o perform very poorly, even falling below the level of random guessing. However, this does not mean that these two models have the worst perceptual and science-related abilities. We observe that these models tend to refuse to answer when they are uncertain, whereas InternVL3 and LLaVA-Onevision randomly guess an answer. For instance, Qwen2.5-VL-72B refused to answer 18,258 questions. This safety mechanism in the models leads to the poor performance of Qwen2.5-VL and GPT-4o.

5 Conclusion

We have introduced OmniEarth-Bench, a foundational multimodal benchmark and the first to establish a systematic evaluation across all six spheres of the Earth system (atmosphere, lithosphere, Ocean-

sphere, cryosphere, biosphere, and human-activity sphere) along with their cross-sphere interactions. This benchmark introduces 109 expert-curated evaluation dimensions and four hierarchical levels of reasoning (perception, general reasoning, expert-knowledge reasoning, and chain-of-thought reasoning), representing a novel and rigorous evaluation design for geoscientific MLLMs. Our results show that even state-of-the-art MLLMs (e.g., Claude) struggle with OmniEarth-Bench; none of the tested models surpassed 35% accuracy. This stark performance gap underscores the benchmark’s difficulty and exposes fundamental limitations in current models’ geoscientific understanding. We anticipate that OmniEarth-Bench will serve as a catalyst for future research in geoscientific AI, guiding the development of models capable of expert-level analysis across Earth’s spheres and enabling advanced applications in environmental monitoring and climate science.

References

- [1] Rami Al-Ruzouq, Mohamed Barakat A Gibril, Abdallah Shanableh, Abubakir Kais, Osman Hamed, Saeed Al-Mansoori, and Mohamad Ali Khalil. Sensors, features, and machine learning for oil spill detection and monitoring: A review. *Remote Sensing*, 12(20):3338, 2020.
- [2] Richard M Allen and Diego Melgar. Earthquake early warning: Advances, scientific challenges, and societal needs. *Annual Review of Earth and Planetary Sciences*, 47(1):361–388, 2019.
- [3] Anthropic. Anthropic ai, 2023. URL <https://www.anthropic.com>.
- [4] Guillaume Astruc, Nicolas Gonthier, Clement Mallet, and Loic Landrieu. Omnisat: Self-supervised modality fusion for earth observation. In *European Conference on Computer Vision*, pp. 409–427. Springer, 2024.
- [5] Shuai Bai, Keqin Chen, Xuejing Liu, Jialin Wang, Wenbin Ge, Sibao Song, Kai Dang, Peng Wang, Shijie Wang, Jun Tang, et al. Qwen2. 5-vl technical report. *arXiv preprint arXiv:2502.13923*, 2025.
- [6] Karianne J Bergen, Paul A Johnson, Maarten V de Hoop, and Gregory C Beroza. Machine learning for data-driven discovery in solid earth geoscience. *Science*, 363(6433):eaau0323, 2019.
- [7] Dagmar Budikova. Role of arctic sea ice in global atmospheric circulation: A review. *Global and Planetary Change*, 68(3):149–163, 2009. ISSN 0921-8181. doi: <https://doi.org/10.1016/j.gloplacha.2009.04.001>. URL <https://www.sciencedirect.com/science/article/pii/S0921818109000654>.
- [8] Yinxia Cao and Qihao Weng. A deep learning-based super-resolution method for building height estimation at 2.5 m spatial resolution in the northern hemisphere. *Remote Sensing of Environment*, 310:114241, 2024.
- [9] Jian Chen, Peilin Zhou, Yining Hua, Dading Chong, Meng Cao, Yaowei Li, Zixuan Yuan, Bing Zhu, and Junwei Liang. Vision-language models meet meteorology: Developing models for extreme weather events detection with heatmaps. *arXiv preprint arXiv:2406.09838*, 2024.
- [10] Zhe Chen, Jiannan Wu, Wenhai Wang, Weijie Su, Guo Chen, Sen Xing, Muyan Zhong, Qinglong Zhang, Xizhou Zhu, Lewei Lu, Bin Li, Ping Luo, Tong Lu, Yu Qiao, and Jifeng Dai. Internvl: Scaling up vision foundation models and aligning for generic visual-linguistic tasks. *arXiv preprint arXiv:2312.14238*, 2023.
- [11] T.R. Chudley, I.M. Howat, M.D. King, et al. Increased crevassing across accelerating greenland ice sheet margins. *Nat. Geosci.*, 18:148–153, 2025. doi: 10.1038/s41561-024-01636-6. URL <https://doi.org/10.1038/s41561-024-01636-6>.
- [12] Josefino Comiso. Bootstrap sea ice concentrations from nimbus-7 smmr and dmsp ssm/i-ssmis, version 4, 2023. URL <http://nsidc.org/data/NSIDC-0079/versions/4>.
- [13] Thomas W Crowther, Henry B Glick, Kristofer R Covey, Charlie Bettigole, Daniel S Maynard, Stephen M Thomas, Jeffrey R Smith, Gregor Hintler, Marlyse C Duguid, Giuseppe Amatulli, et al. Mapping tree density at a global scale. *Nature*, 525(7568):201–205, 2015.

- [14] Qiang Dai, Jingxuan Zhu, Guonian Lv, Latif Kalin, Yuanzhi Yao, Jun Zhang, and Dawei Han. Radar remote sensing reveals potential underestimation of rainfall erosivity at the global scale. *Science advances*, 9(32):eadg5551, 2023.
- [15] Francesca Di Giuseppe, Joe McNorton, Anna Lombardi, and Fredrik Wetterhall. Global data-driven prediction of fire activity. *Nature Communications*, 16(1):2918, 2025.
- [16] Xiaoyi Dong, Pan Zhang, Yuhang Zang, Yuhang Cao, Bin Wang, Linke Ouyang, Xilin Wei, Songyang Zhang, Haodong Duan, Maosong Cao, Wenwei Zhang, Yining Li, Hang Yan, Yang Gao, Xinyue Zhang, Wei Li, Jingwen Li, Kai Chen, Conghui He, Xingcheng Zhang, Yu Qiao, Dahua Lin, and Jiaqi Wang. Internlm-xcomposer2: Mastering free-form text-image composition and comprehension in vision-language large model. *arXiv preprint arXiv:2401.16420*, 2024.
- [17] Zijun Duo, Wenke Wang, and Huizan Wang. Oceanic mesoscale eddy detection method based on deep learning. *Remote Sensing*, 11(16):1921, 2019.
- [18] Matthew Fortier, Mats L Richter, Oliver Sonnentag, and Chris Pal. Carbonsense: A multimodal dataset and baseline for carbon flux modelling. *arXiv preprint arXiv:2406.04940*, 2024.
- [19] Chaoyou Fu, Peixian Chen, Yunhang Shen, Yulei Qin, Mengdan Zhang, Xu Lin, Jinrui Yang, Xiawu Zheng, Ke Li, Xing Sun, et al. Mme: A comprehensive evaluation benchmark for multimodal large language models. *arXiv preprint arXiv:2306.13394*, 2023.
- [20] Timnit Gebru, Jamie Morgenstern, Briana Vecchione, Jennifer Wortman Vaughan, Hanna Wallach, Hal Daumé Iii, and Kate Crawford. Datasheets for datasets. *Communications of the ACM*, 64(12):86–92, 2021.
- [21] Junchao Gong, Lei Bai, Peng Ye, Wanghan Xu, Na Liu, Jianhua Dai, Xiaokang Yang, and Wanli Ouyang. Cascast: Skillful high-resolution precipitation nowcasting via cascaded modelling. *arXiv preprint arXiv:2402.04290*, 2024.
- [22] Yash Goyal, Tejas Khot, Douglas Summers-Stay, Dhruv Batra, and Devi Parikh. Making the v in vqa matter: Elevating the role of image understanding in visual question answering. In *Proceedings of the IEEE conference on computer vision and pattern recognition*, pp. 6904–6913, 2017.
- [23] Zijie Guo, Pumeng Lyu, Fenghua Ling, Lei Bai, Jing-Jia Luo, Niklas Boers, Toshio Yamagata, Takeshi Izumo, Sophie Cravatte, Antonietta Capotondi, et al. Data-driven global ocean modeling for seasonal to decadal prediction. *arXiv preprint arXiv:2405.15412*, 2024.
- [24] Ritwik Gupta, Bryce Goodman, Nirav Patel, Ricky Hosfelt, Sandra Sajeev, Eric Heim, Jigar Doshi, Keane Lucas, Howie Choset, and Matthew Gaston. Creating xbd: A dataset for assessing building damage from satellite imagery. In *Proceedings of the IEEE/CVF conference on computer vision and pattern recognition workshops*, pp. 10–17, 2019.
- [25] Danna Gurari, Qing Li, Abigale J Stangl, Anhong Guo, Chi Lin, Kristen Grauman, Jiebo Luo, and Jeffrey P Bigham. Vizwiz grand challenge: Answering visual questions from blind people. In *Proceedings of the IEEE conference on computer vision and pattern recognition*, pp. 3608–3617, 2018.
- [26] Yoo-Geun Ham, Jeong-Hwan Kim, and Jing-Jia Luo. Deep learning for multi-year ENSO forecasts. *Nature*, 573(7775):568–572, 2019.
- [27] V. Helm, A. Humbert, and H. Miller. Elevation and elevation change of Greenland and Antarctica derived from CryoSat-2. *The Cryosphere*, 8(4):1539–1559, 2014. doi: 10.5194/tc-8-1539-2014. URL <https://tc.copernicus.org/articles/8/1539/2014/>.
- [28] Hans Hersbach, Bill Bell, Paul Berrisford, Shoji Hirahara, András Horányi, Joaquín Muñoz-Sabater, Julien Nicolas, Carole Peubey, Raluca Radu, Dinand Schepers, et al. The ERA5 global reanalysis. *Quarterly journal of the Royal Meteorological Society*, 146(730):1999–2049, 2020.
- [29] Yuan Hu, Jianlong Yuan, Congcong Wen, Xiaonan Lu, and Xiang Li. Rsgpt: A remote sensing vision language model and benchmark. *arXiv preprint arXiv:2307.15266*, 2023.

- [30] Boyin Huang, Peter W Thorne, Viva F Banzon, Tim Boyer, Gennady Chepurin, Jay H Lawrimore, Matthew J Menne, Thomas M Smith, Russell S Vose, and Huai-Min Zhang. Noaa extended reconstructed sea surface temperature (ersst), version 5. (*No Title*), 2017.
- [31] Xingliang Huang, Kaiqiang Chen, Deke Tang, Chenglong Liu, Libo Ren, Zheng Sun, Ronny Hänsch, Michael Schmitt, Xian Sun, Hai Huang, et al. Urban building classification (ubc) v2—a benchmark for global building detection and fine-grained classification from satellite imagery. *IEEE Transactions on Geoscience and Remote Sensing*, 61:1–16, 2023.
- [32] Drew A Hudson and Christopher D Manning. Gqa: A new dataset for real-world visual reasoning and compositional question answering. In *Proceedings of the IEEE/CVF conference on computer vision and pattern recognition*, pp. 6700–6709, 2019.
- [33] Dongzhi Jiang, Renrui Zhang, Ziyu Guo, Yanwei Li, Yu Qi, Xinyan Chen, Liuhui Wang, Jianhan Jin, Claire Guo, Shen Yan, et al. Mme-cot: Benchmarking chain-of-thought in large multimodal models for reasoning quality, robustness, and efficiency. *arXiv preprint arXiv:2502.09621*, 2025.
- [34] S Kainkaryam, C Ong, S Sen, and A Sharma. Crowdsourcing salt model building: Kaggle-tgs salt identification challenge. In *81st EAGE Conference and Exhibition 2019*, pp. 1–5. European Association of Geoscientists & Engineers, 2019.
- [35] S.A. Khan, Y. Choi, M. Morlighem, et al. Extensive inland thinning and speed-up of northeast greenland ice stream. *Nature*, 611:727–732, 2022. doi: 10.1038/s41586-022-05301-z. URL <https://doi.org/10.1038/s41586-022-05301-z>.
- [36] Katerina Kikaki, Ioannis Kakogeorgiou, Ibrahim Hoteit, and Konstantinos Karantzalos. Detecting marine pollutants and sea surface features with deep learning in sentinel-2 imagery. *ISPRS Journal of Photogrammetry and Remote Sensing*, 2024.
- [37] Asanobu Kitamoto, Jared Hwang, Bastien Vuillod, Lucas Gautier, Yingtao Tian, and Tarin Clanuwat. Digital typhoon: Long-term satellite image dataset for the spatio-temporal modeling of tropical cyclones. *Advances in Neural Information Processing Systems*, 36:40623–40636, 2023.
- [38] Darko Koračin, Clive E Dorman, John M Lewis, James G Hudson, Eric M Wilcox, and Alicia Torregrosa. Marine fog: A review. *Atmospheric research*, 143:142–175, 2014.
- [39] Kartik Kuckreja, Muhammad Sohail Danish, Muzammal Naseer, Abhijit Das, Salman Khan, and Fahad Shahbaz Khan. Geochat: Grounded large vision-language model for remote sensing. In *Proceedings of the IEEE/CVF Conference on Computer Vision and Pattern Recognition*, pp. 27831–27840, 2024.
- [40] Bo Li, Peiyuan Zhang, Kaichen Zhang, Fanyi Pu, Xinrun Du, Yuhao Dong, Haotian Liu, Yuanhan Zhang, Ge Zhang, Chunyuan Li, and Ziwei Liu. Lmms-eval: Accelerating the development of large multimodal models. <https://github.com/EvolvingLMms-Lab/lmms-eval>, March 2024. URL <https://github.com/EvolvingLMms-Lab/lmms-eval>.
- [41] Bo Li, Yuanhan Zhang, Dong Guo, Renrui Zhang, Feng Li, Hao Zhang, Kaichen Zhang, Yanwei Li, Ziwei Liu, and Chunyuan Li. Llava-onevision: Easy visual task transfer. *arXiv preprint arXiv:2408.03326*, 2024.
- [42] Bohao Li, Rui Wang, Guangzhi Wang, Yuying Ge, Yixiao Ge, and Ying Shan. Seed-bench: Benchmarking multimodal llms with generative comprehension. *arXiv preprint arXiv:2307.16125*, 2023.
- [43] Haobo Li, Zhaowei Wang, Jiachen Wang, Alexis Kai Hon Lau, and Huamin Qu. Cllmate: A multimodal llm for weather and climate events forecasting. *arXiv preprint arXiv:2409.19058*, 2024.
- [44] Jiayi Li, Xin Huang, and Lilin Tu. Whu-ohs: A benchmark dataset for large-scale hersepectral image classification. *International Journal of Applied Earth Observation and Geoinformation*, 113:103022, 2022.

- [45] Qingmei Li, Yang Zhang, Zurong Mai, Yuhang Chen, Shuohong Lou, Henglian Huang, Jiarui Zhang, Zhiwei Zhang, Yibin Wen, Weijia Li, et al. Can large multimodal models understand agricultural scenes? benchmarking with agromind. *arXiv preprint arXiv:2505.12207*, 2025.
- [46] Xiang Li, Jian Ding, and Mohamed Elhoseiny. Vrsbench: A versatile vision-language benchmark dataset for remote sensing image understanding. *arXiv preprint arXiv:2406.12384*, 2024.
- [47] Shunlin Liang, Jie Cheng, Kun Jia, Bo Jiang, Qiang Liu, Zhiqiang Xiao, Yunjun Yao, Wenping Yuan, Xiaotong Zhang, Xiang Zhao, et al. The global land surface satellite (glass) product suite. *Bulletin of the American Meteorological Society*, 102(2):E323–E337, 2021.
- [48] Fenghua Ling, Jing-Jia Luo, Yue Li, Tao Tang, Lei Bai, Wanli Ouyang, and Toshio Yamagata. Multi-task machine learning improves multi-seasonal prediction of the indian ocean dipole. *Nature Communications*, 13(1):7681, 2022.
- [49] Jun Liu, Youmin Tang, Yanling Wu, Tang Li, Qiang Wang, and Dake Chen. Forecasting the indian ocean dipole with deep learning techniques. *Geophysical Research Letters*, 48(20):e2021GL094407, 2021.
- [50] Yuan Liu, Haodong Duan, Yuanhan Zhang, Bo Li, Songyang Zhang, Wangbo Zhao, Yike Yuan, Jiaqi Wang, Conghui He, Ziwei Liu, et al. Mmbench: Is your multi-modal model an all-around player? In *European conference on computer vision*, pp. 216–233. Springer, 2024.
- [51] Junwei Luo, Yingying Zhang, Xue Yang, Kang Wu, Qi Zhu, Lei Liang, Jingdong Chen, and Yansheng Li. When large vision-language model meets large remote sensing imagery: Coarse-to-fine text-guided token pruning. *arXiv preprint arXiv:2503.07588*, 2025.
- [52] Chengqian Ma, Zhanxiang Hua, Alexandra Anderson-Frey, Vikram Iyer, Xin Liu, and Lianhui Qin. Weatherqa: Can multimodal language models reason about severe weather? *arXiv preprint arXiv:2406.11217*, 2024.
- [53] Xiaogang Ma. Data science for geoscience: Recent progress and future trends from the perspective of a data life cycle. 2023.
- [54] Kenneth Marino, Mohammad Rastegari, Ali Farhadi, and Roozbeh Mottaghi. Ok-vqa: A visual question answering benchmark requiring external knowledge. In *Proceedings of the IEEE/cvf conference on computer vision and pattern recognition*, pp. 3195–3204, 2019.
- [55] Ahmed Masry, Do Xuan Long, Jia Qing Tan, Shafiq Joty, and Enamul Hoque. Chartqa: A benchmark for question answering about charts with visual and logical reasoning. *arXiv preprint arXiv:2203.10244*, 2022.
- [56] W.N. Meier, F. Fetterer, A.K. Windnagel, and J.S. Stewart. Noaa/nsidc climate data record of passive microwave sea ice concentration. (g02202, version 4). *National Snow and Ice Data Center*, 2021. doi: <https://doi.org/10.7265/efmz-2t65>.
- [57] S Mostafa Mousavi, Yixiao Sheng, Weiqiang Zhu, and Gregory C Beroza. Stanford earthquake dataset (stead): A global data set of seismic signals for ai. *IEEE Access*, 7:179464–179476, 2019.
- [58] Dilxat Muhtar, Zhenshi Li, Feng Gu, Xueliang Zhang, and Pengfeng Xiao. Lhrs-bot: Empowering remote sensing with vgi-enhanced large multimodal language model. In *European Conference on Computer Vision*, pp. 440–457. Springer, 2024.
- [59] Daniyar B Nurseitov, Galymzhan Abdimanap, Abdelrahman Abdallah, Gulshat Sagatdinova, Larissa Balakay, Tatyana Dedova, Nurkuisa Rametov, and Anel Alimova. Rosid: Remote sensing satellite data for oil spill detection on land. *Engineered Science*, 32:1348, 2024.
- [60] Daniyar B Nurseitov, Galymzhan Abdimanap, Abdelrahman Abdallah, Gulshat Sagatdinova, Larissa Balakay, Tatyana Dedova, Nurkuisa Rametov, and Anel Alimova. Rosid: Remote sensing satellite data for oil spill detection on land. *Engineered Science*, 32:1348, 2024.
- [61] OpenAI. Hello gpt-4o. <https://openai.com/index/hello-gpt-4o>, 2024.

- [62] Long Phan, Alice Gatti, Ziwen Han, Nathaniel Li, Josephina Hu, Hugh Zhang, Chen Bo Calvin Zhang, Mohamed Shaaban, John Ling, Sean Shi, et al. Humanity’s last exam. *arXiv preprint arXiv:2501.14249*, 2025.
- [63] Yifei Qian, Grant RW Humphries, Philip N Trathan, Andrew Lowther, and Carl R Donovan. Counting animals in aerial images with a density map estimation model. *Ecology and Evolution*, 13(4):e9903, 2023.
- [64] Markus Reichstein, Gustau Camps-Valls, Bjorn Stevens, Martin Jung, Joachim Denzler, Nuno Carvalhais, and F Prabhat. Deep learning and process understanding for data-driven earth system science. *Nature*, 566(7743):195–204, 2019.
- [65] Jonathan Roberts, Mohammad Reza Taesiri, Ansh Sharma, Akash Gupta, Samuel Roberts, Ioana Croitoru, Simion-Vlad Bogolin, Jialu Tang, Florian Langer, Vyas Raina, et al. Zerobench: An impossible visual benchmark for contemporary large multimodal models. *arXiv preprint arXiv:2502.09696*, 2025.
- [66] Tanik Saikh, Tirthankar Ghosal, Amish Mittal, Asif Ekbal, and Pushpak Bhattacharyya. Scienceqa: A novel resource for question answering on scholarly articles. *International Journal on Digital Libraries*, 23(3):289–301, 2022.
- [67] Eric W Sanderson, Malanding Jaiteh, Marc A Levy, Kent H Redford, Antoinette V Wannebo, and Gillian Woolmer. The human footprint and the last of the wild: the human footprint is a global map of human influence on the land surface, which suggests that human beings are stewards of nature, whether we like it or not. *BioScience*, 52(10):891–904, 2002.
- [68] Srikumar Sastry, Subash Khanal, Aayush Dhakal, Adeel Ahmad, and Nathan Jacobs. Taxabind: A unified embedding space for ecological applications. In *2025 IEEE/CVF Winter Conference on Applications of Computer Vision (WACV)*, pp. 1765–1774. IEEE, 2025.
- [69] Axel Schweiger, Ronald Lindsay, Jinlun Zhang, Michael Steele, and H Stern. Uncertainty in modeled arctic sea ice volume. *Journal of Geophysical Research*, 116(C00D06):1–15, 2011. doi: 10.1029/2011JC007084.
- [70] Amanpreet Singh, Vivek Natarajan, Meet Shah, Yu Jiang, Xinlei Chen, Dhruv Batra, Devi Parikh, and Marcus Rohrbach. Towards vqa models that can read. In *Proceedings of the IEEE/CVF conference on computer vision and pattern recognition*, pp. 8317–8326, 2019.
- [71] Ben Smith, Susheel Adusumilli, Be??ta Csathó, Denis Felikson, Helen Fricker, Alex Gardner, Nick Holschuh, Jeff Lee, Johan Nilsson, Fernando Paolo, Matthew Siegfried, Tyler Sutterley, and The ICESat-2 Science Team. Atlas/icesat-2 l3a land ice height, version 6, 2023. URL <http://nsidc.org/data/ATL06/versions/6>.
- [72] Sagar Soni, Akshay Dudhane, Hiyam Debary, Mustansar Fiaz, Muhammad Akhtar Munir, Muhammad Sohail Danish, Paolo Fraccaro, Campbell D Watson, Levente J Klein, Fahad Shahbaz Khan, et al. Earthdial: Turning multi-sensory earth observations to interactive dialogues. In *Proceedings of the Computer Vision and Pattern Recognition Conference*, pp. 14303–14313, 2025.
- [73] Jason Stock, Kyle Hilburn, Imme Ebert-Uphoff, and Charles Anderson. Srvit: Vision transformers for estimating radar reflectivity from satellite observations at scale. *arXiv preprint arXiv:2406.16955*, 2024.
- [74] Michael Studinger. Icebridge atm l2 icesn elevation, slope, and roughness, version 2, 2014. URL <http://nsidc.org/data/ILATM2/versions/2>.
- [75] Yuxi Sun, Shanshan Feng, Xutao Li, Yunming Ye, Jian Kang, and Xu Huang. Visual grounding in remote sensing images. In *Proceedings of the 30th ACM International Conference on Multimedia*, pp. 404–412, 2022.
- [76] James Super. Geoscientists excluded. *Nature Geoscience*, 16(3):194–194, 2023.

- [77] Gemini Team, Rohan Anil, Sebastian Borgeaud, Yonghui Wu, Jean-Baptiste Alayrac, Jiahui Yu, Radu Soricut, Johan Schalkwyk, Andrew M Dai, Anja Hauth, et al. Gemini: a family of highly capable multimodal models. *arXiv preprint arXiv:2312.11805*, 2023.
- [78] Mélisande Teng, Amna Elmustafa, Benjamin Akera, Yoshua Bengio, Hager Radi, Hugo Larochelle, and David Rolnick. Satbird: a dataset for bird species distribution modeling using remote sensing and citizen science data. *Advances in Neural Information Processing Systems*, 36:75925–75950, 2023.
- [79] Axel Timmermann, Soon-Il An, Jong-Seong Kug, Fei-Fei Jin, Wenju Cai, Antonietta Capotondi, Kim M Cobb, Matthieu Lengaigne, Michael J McPhaden, Malte F Stuecker, et al. El niño–southern oscillation complexity. *Nature*, 559(7715):535–545, 2018.
- [80] Peter Tong, Ellis Brown, Penghao Wu, Sanghyun Woo, Adithya Jairam Vedagiri IYER, Sai Charitha Akula, Shusheng Yang, Jihan Yang, Manoj Middepogu, Ziteng Wang, et al. Cambrian-1: A fully open, vision-centric exploration of multimodal llms. *Advances in Neural Information Processing Systems*, 37:87310–87356, 2024.
- [81] Mark Veillette, Siddharth Samsi, and Chris Mattioli. Sevir: A storm event imagery dataset for deep learning applications in radar and satellite meteorology. In *Advances in Neural Information Processing Systems*, volume 33, pp. 22009–22019, 2020.
- [82] Josh Veitch-Michaelis, Andrew Cottam, Daniella Schweizer, Eben Broadbent, David Dao, Ce Zhang, Angelica Almeyda Zambrano, and Simeon Max. Oam-tcd: A globally diverse dataset of high-resolution tree cover maps. *Advances in Neural Information Processing Systems*, 37:49749–49767, 2024.
- [83] Oscar Venter, Eric W Sanderson, Ainhoa Magrath, James R Allan, Jutta Beher, Kendall R Jones, Hugh P Possingham, William F Laurance, Peter Wood, Balázs M Fekete, et al. Sixteen years of change in the global terrestrial human footprint and implications for biodiversity conservation. *Nature communications*, 7(1):12558, 2016.
- [84] Eric Vermote. Mod09a1 modis/terra surface reflectance 8-day l3 global 500m sin grid v006, 2015. URL <https://doi.org/10.5067/MODIS/MOD09A1.006>.
- [85] Brandon Victor, Mathilde Letard, Peter Naylor, Karim Douch, Nicolas Longépé, Zhen He, and Patrick Ebel. Off to new shores: A dataset & benchmark for (near-) coastal flood inundation forecasting. *Advances in Neural Information Processing Systems*, 37:114797–114811, 2024.
- [86] Fengxiang Wang, Hongzhen Wang, Mingshuo Chen, Di Wang, Yulin Wang, Zonghao Guo, Qiang Ma, Long Lan, Wenjing Yang, Jing Zhang, et al. Xlrs-bench: Could your multimodal llms understand extremely large ultra-high-resolution remote sensing imagery? *arXiv preprint arXiv:2503.23771*, 2025.
- [87] Lizhe Wang, Boxin Zuo, Yuan Le, Yifu Chen, and Jun Li. Penetrating remote sensing: Next-generation remote sensing for transparent earth. *The Innovation*, 4(6), 2023.
- [88] Peng Wang, Shuai Bai, Sinan Tan, Shijie Wang, Zhihao Fan, Jinze Bai, Keqin Chen, Xuejing Liu, Jialin Wang, Wenbin Ge, et al. Qwen2-vl: Enhancing vision-language model’s perception of the world at any resolution. *arXiv preprint arXiv:2409.12191*, 2024.
- [89] Yan Wang, Ge Chen, Jie Yang, Zhipeng Gui, and Dehua Peng. A submesoscale eddy identification dataset in the northwest pacific ocean derived from goci i chlorophyll a data based on deep learning. *Earth System Science Data*, 16(12):5737–5752, 2024.
- [90] Kaining Ying, Fanqing Meng, Jin Wang, Zhiqian Li, Han Lin, Yue Yang, Hao Zhang, Wenbo Zhang, Yuqi Lin, Shuo Liu, et al. Mmt-bench: A comprehensive multimodal benchmark for evaluating large vision-language models towards multitask agi. In *International Conference on Machine Learning*, pp. 57116–57198. PMLR, 2024.
- [91] Siwei Yu and Jianwei Ma. Deep learning for geophysics: Current and future trends. *Reviews of Geophysics*, 59(3):e2021RG000742, 2021.

- [92] Xiang Yue, Tianyu Zheng, Yuansheng Ni, Yubo Wang, Kai Zhang, Shengbang Tong, Yuxuan Sun, Botao Yu, Ge Zhang, Huan Sun, et al. Mmmu-pro: A more robust multi-discipline multimodal understanding benchmark. *arXiv preprint arXiv:2409.02813*, 2024.
- [93] Yang Zhan, Zhitong Xiong, and Yuan Yuan. Rsvg: Exploring data and models for visual grounding on remote sensing data. *IEEE Transactions on Geoscience and Remote Sensing*, 61: 1–13, 2023.
- [94] Jinlun Zhang and D.A. Rothrock. Modeling global sea ice with a thickness and enthalpy distribution model in generalized curvilinear coordinates. *Monthly Weather Review*, 131(5): 681–697, 2003.
- [95] Kaichen Zhang, Bo Li, Peiyuan Zhang, Fanyi Pu, Joshua Adrian Cahyono, Kairui Hu, Shuai Liu, Yuanhan Zhang, Jingkang Yang, Chunyuan Li, and Ziwei Liu. Lmms-eval: Reality check on the evaluation of large multimodal models. *arXiv preprint arXiv:2407.12772*, 2024.
- [96] Pan Zhang, Xiaoyi Dong, Yuhang Zang, Yuhang Cao, Rui Qian, Lin Chen, Qipeng Guo, Haodong Duan, Bin Wang, Linke Ouyang, et al. Internlm-xcomposer-2.5: A versatile large vision language model supporting long-contextual input and output. *arXiv preprint arXiv:2407.03320*, 2024.
- [97] Wei Zhang, Miaoxin Cai, Tong Zhang, Yin Zhuang, and Xuerui Mao. Earthgpt: A universal multi-modal large language model for multi-sensor image comprehension in remote sensing domain. *IEEE Transactions on Geoscience and Remote Sensing*, 2024.
- [98] Yi-Fan Zhang, Huanyu Zhang, Haochen Tian, Chaoyou Fu, Shuangqing Zhang, Junfei Wu, Feng Li, Kun Wang, Qingsong Wen, Zhang Zhang, et al. Mme-realworld: Could your multimodal llm challenge high-resolution real-world scenarios that are difficult for humans? *arXiv preprint arXiv:2408.13257*, 2024.
- [99] Juepeng Zheng, Haohuan Fu, Weijia Li, Wenzhao Wu, Le Yu, Shuai Yuan, Wai Yuk William Tao, Tan Kian Pang, and Kasturi Devi Kanniah. Growing status observation for oil palm trees using unmanned aerial vehicle (uav) images. *ISPRS Journal of Photogrammetry and Remote Sensing*, 173:95–121, 2021.
- [100] Juepeng Zheng, Haohuan Fu, Weijia Li, Wenzhao Wu, Le Yu, Shuai Yuan, Wai Yuk William Tao, Tan Kian Pang, and Kasturi Devi Kanniah. Growing status observation for oil palm trees using unmanned aerial vehicle (uav) images. *ISPRS Journal of Photogrammetry and Remote Sensing*, 173:95–121, 2021.
- [101] Wei Zhi, Alison P Appling, Heather E Golden, Joel Podgorski, and Li Li. Deep learning for water quality. *Nature water*, 2(3):228–241, 2024.
- [102] Baichuan Zhou, Haote Yang, Dairong Chen, Junyan Ye, Tianyi Bai, Jinhua Yu, Songyang Zhang, Dahua Lin, Conghui He, and Weijia Li. Urbench: A comprehensive benchmark for evaluating large multimodal models in multi-view urban scenarios. *Proceedings of the AAAI Conference on Artificial Intelligence*, 39(10):10707–10715, 2025.
- [103] W. Zhou, L.R. Leung, and J. Lu. Steady threefold arctic amplification of externally forced warming masked by natural variability. *Nat. Geosci.*, 17:508–515, 2024. doi: 10.1038/s41561-024-01441-1. URL <https://doi.org/10.1038/s41561-024-01441-1>.
- [104] Jinguo Zhu, Weiyun Wang, Zhe Chen, Zhaoyang Liu, Shenglong Ye, Lixin Gu, Yuchen Duan, Hao Tian, Weijie Su, Jie Shao, et al. Internvl3: Exploring advanced training and test-time recipes for open-source multimodal models. *arXiv preprint arXiv:2504.10479*, 2025.

A Appendix

A.1 Overview of the Appendix

This appendix supplements the proposed **OmniEarth-Bench** with details excluded from the main paper due to space constraints. The appendix is organized as follows:

- Sec. A.2: More details of OmniEarth-Bench.
- Sec. A.3: Data Processing Strategies for each Spheres.
- Sec. A.4: Construction Details of Different Question Formats.
- Sec. A.5: Detailed results of specific sub-tasks (L-4 dimension).
- Sec. A.6: Detailed results of specific sub-tasks (L-3 dimension).
- Sec. A.7: Visualizations of samples and challenging cases.
- Sec. A.8: Datasheets for the OmniEarth-Bench dataset.
- Sec. A.9: Discussion on limitations and societal impact.
- Sec. A.9: Usage of LLM.

A.2 More Details of OmniEarth-Bench

This section provides additional details about the dataset. We begin with a visual illustration (Fig.4) that highlights the structure and real-world applicability of OmniEarth-Bench, presenting a curated example from each scientific sphere to show how the benchmark spans from high-level domains (L1) down to specific, expert-defined tasks (L4). To complement this overview, Table 8 and Table 9 present detailed statistics for each L4 dimension, along with their relationships to the L3 and L2 dimensions, fully clarifying the dataset’s structure and composition.

Experiments setup. Following MMBench [50] and MME-Realworld [98] methods, in the MCQ format of the VQA task, we manually created 5 options for each question: one correct answer, three distractors, and one special answer (unable to answer). We evaluated the accuracy and reported the L-1 dimension for the VQA task, with L-3 and L-4 results available in the Appendix A.5 and Appendix A.6. All scores in Tab. 4 are reported as percentages (%). For the Grounding task, we used precision, assessing accuracy based on the intersection between predicted and ground truth bounding boxes, with predictions deemed correct if IoU exceeds a threshold (0.5 and 0.7). For open-ended evaluation, we use an external LLM as a judge to automatically assess the correctness of the generated answers. Following the XLRs-Bench [86], to evaluate the quality of the generated captions, we employed a comprehensive suite of standard metrics, including BLEU, METEOR, ROUGE_L, and CIDEr.

Human Annotations vs. GPT Annotations. All annotations are finished by experts and crowd-sourcing annotators. Unlike MMBench [50], we did not use tools like GPT-4o [61]. It was driven by two key reasons: (1) GPT-4o cannot generate VQA data requiring deep domain expertise. Tasks under the Scientific-Knowledge Reasoning (L3) demand substantial background knowledge and must be constructed collaboratively by experts. (2) Although GPT-4o can generate samples for general perception or simple reasoning tasks, expert evaluation found the data to be low quality and insufficiently challenging. For example, in the visual grounding task, GPT-4o only detects highly salient structures, failing to support our goal of testing MLLMs on locating diverse buildings across complex scenes. As a result, all OmniEarth-Bench data was exclusively created by experts and annotators.

A.2.1 Cross-sphere

- L2-Global Flood Forecasting:
 - **Flood Detecting:** Predicts whether a flood event will occur in the near future based on ground and atmospheric variables, including river discharge, 2-meter air temperature, top-layer volumetric soil water content, snow depth water equivalent, total precipitation, along with Sentinel VV / VH data from the preceding two days.

- **Flood Predicting:** Predicts whether a flood event will occur in the near future based on the same variables used in Flood Detecting, along with Sentinel VV / VH data from the preceding two days.
- L2-Carbon flux monitoring:
 - **Carbon flux estimation:** Refers to the process of quantifying the rate and direction of carbon exchange (e.g., carbon dioxide) between the biosphere (vegetation and microorganisms, etc.) and the atmosphere, which tests the LLM’s ability to interpret biogeochemical cycles, integrate multi-dimensional environmental data (e.g., satellite, sensor networks), and apply physics-based or statistical models for climate change analysis.
- L2-Bird species prediction:
 - **Most likely species to occur:** Predicting the species with the highest likelihood of presence in a specific habitat based on environmental variables (e.g., climate, habitat type), testing the LLM’s ability to analyze spatial-environmental correlations and prioritize species under data-driven constraints.
 - **Species occurrence probability estimation:** Quantifying the probability of a species being present in a given geographic area, evaluating the LLM’s grasp of probabilistic reasoning and ecological variable weighting.
 - **Species richness estimation:** Calculating the total number of distinct species within a defined ecosystem or region, testing the LLM’s capacity to integrate multi-modal data to predict biodiversity.

A.2.2 Human-activity sphere

The human-activity sphere leverages remote sensing and mapping technologies across three key scenarios: *Urban Construction (L2)*, *Land Use (L2)*, and *Surface Disaster Assessment (L2)*. Urban construction supports planning and socio-economic analysis; land use classification underpins environmental monitoring and resource management; and disaster assessment enables rapid post-event response and risk mitigation. OmniEarth-Bench spans all four L3 capability dimensions in the human-activity sphere—Perception, General Reasoning, Scientific-Knowledge Reasoning, and CoT Reasoning—with **27 subtasks (L4 dimensions)**, surpassing all existing benchmarks in this domain [46, 86]. The complete task details are as follows.

- L2-Surface Disaster Assessment:
 - **Change detection counting of post-disaster completely destroyed building:** Compares pre- and post-disaster images to count fully destroyed buildings, evaluating temporal change detection.
 - **Counting of post-disaster partially damaged building:** Detects and counts lightly or moderately damaged structures in post-disaster imagery.
 - **Building damage prediction:** Estimates potential damage severity from pre-disaster views, testing risk assessment without ground truth.
 - **Disaster prediction:** Predicts future disaster types using current imagery, evaluating temporal modeling capabilities.
 - **Disaster type classification:** Identifies disaster types (e.g., flood, earthquake) from satellite images, testing visual pattern recognition.
 - **Geolocation estimation of disaster-affected regions from imagery:** Predicts the geographic location of affected areas based on visual cues, assessing spatial referencing.
 - **Individual building damage assessment:** Compares pre- and post-event imagery to evaluate building-level structural changes.
 - **Multi-image individual visual localization task:** Uses multi-temporal or multi-view images to locate specific buildings, assessing multi-view reasoning.
 - **Spatial relationships under complex conditions:** Infers spatial relations (e.g., relative position, containment) between objects in imagery, testing 3D reasoning.
 - **Visual grounding of damaged individual buildings:** Locates damaged structures in post-disaster imagery, evaluating anomaly detection and spatial precision.
- L2-Urban Development:

- **Fine-grained object type recognition:** Classifies specified buildings in high-resolution imagery, testing the model’s ability to distinguish visually similar structures.
- **Overall counting:** Counts all buildings or urban facilities in an image, evaluating object detection and counting under complex conditions.
- **Counting under complex conditions:** Counts objects that meet given conditions (e.g., attributes or constraints), testing constrained multimodal reasoning.
- **Overall building height estimation:** Estimates structural vertical dimensions using multi-source geospatial inputs, assessing 3D reconstruction accuracy and cross-sensor measurement consistency.
- **Individual building height estimation:** Estimates the height of an individual building from satellite views, testing 2D-to-3D inference.
- L2-Land Use:
 - **Overall land type classification:** Identifies macro land cover types (e.g., urban, farmland, water), evaluating scene-level understanding.
 - **Fine-grained land type classification:** Classifies specific land use (e.g., crop types) at finer scales, testing detailed semantic discrimination.
 - **Visual localization of land use types:** Locates specific land types within an image, evaluating spatial perception.
 - **Counting of land types under complex conditions:** Counts land use regions meeting complex conditions, assessing constrained visual reasoning.
 - **Visual grouping of land types:** Locates specific land types to evaluate the model’s visual localization capability and land type classification ability.

A.2.3 Biosphere

We present a biosphere-focused MLLM benchmark built on observational data and retrieval products, featuring **15 practical L4 subtasks**. It includes four representative L2 scenarios: Vegetation Monitoring (L2), Human Footprint Assessment (L2), Environmental Pollution Monitoring (L2), Species Distribution Prediction (L2), and Crop Growth Monitoring (L2). Vegetation Monitoring [13] evaluates plant and ecosystem health to support function assessment, carbon accounting, and climate response. Human Footprint Assessment [83] quantifies human impact on nature, informing sustainability and biodiversity strategies. Environmental Pollution Monitoring [60] identifies pollution events and their extent, guiding environmental policy and mitigation. Species Distribution is a key concern in the biosphere, as it guides biodiversity conservation and supports modeling species range shifts under climate and land-use change. Crop Growth Monitoring [100] assesses crop health for precision agriculture and sustainable farming. The complete task details are as follows.

- L2-Crop growth monitoring:
 - **Dead oil palm identification:** Identifies dead trees in unmanned aerial vehicle (UAV) imagery, testing the model’s domain knowledge in crop growth.
 - **Dead oil palm counting:** Counting the number of dead trees in an image, testing the model’s object counting capability.
- L2-Environmental pollution monitoring:
 - **Terrestrial oil spill counting:** Counting oil spill points in satellite imagery, testing the model’s ability in environmental pollution recognition and object counting.
 - **Terrestrial oil spill area calculation:** Calculating the total area of oil spills in the image, evaluating the model’s applicability in pollution events.
- L2-Human footprint assessment:
 - **Human footprint assessment:** Assessing the impact of human activities in the region based on imagery, testing the model’s ability to recognize and reason about human activity features
 - **Human footprint index estimation:** Calculating the human footprint index of a region, testing the model’s understanding of human activity patterns.
- L2-Species Distribution Prediction:

- **Tree species prediction:** Identifying the type of tree that occupies the largest proportion, testing the model’s ability to recognize features of different tree species.
- **Tree species proportion prediction:** Identifying the proportion of specific tree species, testing the model’s ability in species recognition and statistical reasoning.
- **Animal classification:** Identifying animal species within the bounding box, testing the model’s ability to extract local information and distinguish between different animal species.
- **Geographical location inference of plant species:** Inferring the geographic coordinates from the image and the given tree species, testing the model’s domain knowledge of tree species distribution.
- **Global animal counting:** Counting the number of animals in the image, testing the model’s ability in animal instance extraction and counting.
- **Species distribution prediction:** Predicting the likely animal species in a region based on the image and geographic coordinates, testing the model’s ability to extract ecological features and its knowledge of species distribution.
- L2-Vegetation monitoring:
 - **Fractional vegetation cover estimation:** Calculating the fractional vegetation cover in the image, testing the model’s ability to recognize vegetation features.
 - **Leaf area index estimation:** Calculating the leaf area index from multi-band imagery, testing the model’s ability to comprehensively understand and utilize multi-source information.
 - **Peak vegetation coverage area grounding:** Locating peak vegetation coverage areas in the image using multi-band imagery, testing the model’s ability to localize vegetation features.

A.2.4 Atmosphere

The atmosphere is a key domain in Earth sciences with high practical value and extensive research interest [21, 73]. While existing benchmarks target specific atmospheric sub-scenarios [52, 9, 43], they lack comprehensive domain-wide coverage. OmniEarth-Bench addresses this gap by defining evaluation dimensions across six representative scenarios using data from ERA5 [28], SEVIR [81], and Typhoon [37] datasets: *Short-term Weather Events (L2)*, *Medium-term Weather Events (L2)*, *Seasonal Weather Events (L2)*, *Interannual Climate Variation (L2)*, *Typhoon Event (L2)*, and *SEVIR Weather (L2)*. For example, the *Typhoon Event* dimension serves as a flagship benchmark for atmospheric machine learning, supporting operational hazard forecasting and advancing research on tropical cyclone intensity and structure. These six scenarios (L2) span **36 expert-designed subtasks (L4 dimensions)** with strong real-world relevance, substantially surpassing existing atmospheric benchmarks. The complete task details are as follows.

- L2-Short-term weather events:
 - **Event intensity identification:**Determine extreme intensity or variable value at given position or region.
 - **Event localization:**Localize event center or moving direction of event.
 - **Event trend analysis:**Determine varying trend or speed of variable.
 - **Event type identification:**Determine type of current event.
 - **Dynamic feature identification:**Determine dynamic structure via multi-variable analysis.
 - **Event evolution analysis:**Determine stage of event via multi-variable analysis.
 - **Thermodynamic feature identification:**Determine thermodynamic features or structure via multi-variable analysis.
- L2-Medium-term weather events:
 - **Cyclone movement identification:** Determine moving direction of cyclone.
 - **Cyclone phase identification:** Determine the different phase of cyclone
 - **Event intensity identification:** Determine extreme intensity or variable value at given position or region.

- **Event localization:** Localize event center or moving direction of event.
- **Event trend analysis:** Determine varying speed or trend of current event.
- **Geopotential pattern identification:** Determine pattern / structure of given geopotential.
- **Moisture flux analysis:** Determine intensity of moisture flux transformation.
- **System identification:** Determine dynamic structure via multi-variable analysis.
- **System evolution trend analysis:** Determine the evolution stage of the current system via multi-variable analysis.
- L2-Typhoon:
 - **Pressure estimation:** Using the same image stacks, the task outputs the minimum sea-level pressure (hPa) at the cyclone eye; this complements wind speed and enables pressure–wind relationship validation.
 - **Radius of major gale axis estimation:** Using scatterometer-derived peak-gust layers, the model regresses the semi-major radius (km) of 50-kt gusts, characterising the reach of damaging winds for early warning.
 - **Radius of major storm axis estimation:** From the segmented wind-field map, the model estimates the semi-major radius (km) of 34-kt gale-force winds, quantifying the storm’s main spatial extent and directly supporting surge-risk assessment.
 - **Radius of minor gale axis estimation:** Outputs the corresponding semi-minor radius, enabling a complete 2-D description of the gust envelope.
 - **Radius of minor storm axis estimation:** Analogous to the above, but for the semi-minor radius, capturing asymmetric size features critical to track-shift sensitivity analysis.
 - **Wind estimation:** Given time-synchronised multispectral satellite images, models must regress the storm-centre 1-min sustained surface wind speed in kt, providing a physics-consistent proxy for Saffir–Simpson intensity classification.
- L2-Seasonal weather events:
 - **Precipitation anomaly identification:** Determine precipitation anomaly value at given timestamp or region.
 - **Seasonal comparison:** Analysis of temperature/precipitation anomaly within a year.
 - **Temperature anomaly identification:** Determine temperature anomaly value at given timestamp or region.
- L2-Interannual climate variation:
 - **ENSO feature analysis:** Determine status or features of ENSO.
 - **Long-term Precipitation trend analysis:** Determine trend of precipitation anomaly among years.
 - **Long-term Temperature trend identification:** Determine trend of temperature anomaly among years.
- L2-SEVIR Weather:
 - **Event type prediction:** Identifies storm event types based on visible and infrared channels from satellite, along with Vertical Integrated Liquid (VIL) data from weather radar.
 - **Miss alarm estimation:** Estimates the miss rate by comparing forecasted outputs against SEVIR ground truth.
 - **Movement prediction:** Given a sequence of VIL data, MLLMs are required to identify the move direction of the convective system.
 - **Rotate center prediction**

A.2.5 Lithosphere

We firstly construct an MLLM benchmark for the lithosphere based on observational data, comprising **8 practical subtasks (L4 dimensions)** . We define two representative L2 scenarios within the lithosphere: *Seismic Monitoring and Prediction (L2)* and *Geophysical Exploration (L2)*. Seismic monitoring and prediction [2], a critical domain in geosciences, aims to uncover Earth’s internal

dynamics and earthquake nucleation mechanisms, forming a theoretical basis for early warning and disaster mitigation. Geophysical exploration imaging [91], by analyzing subsurface responses to physical fields such as seismic waves, electromagnetic fields, and gravity/magnetic anomalies, enables high-resolution geological modeling essential for understanding subsurface structures, hydrocarbon exploration, and geological hazard assessment. The complete task details are as follows.

- L2-Earthquake monitoring and prediction:
 - **P-wave phase picking:** Taking three-component observed seismic waveforms as input, output the arrival times of the P-wave characteristic seismic signals.
 - **S-wave phase picking:** Taking three-component observed seismic waveforms as input, output the arrival times of the S-wave characteristic seismic signals.
 - **Earthquake or noise classification:** Distinguishing seismic signals from natural earthquakes versus artificial noise or vibrations, testing the LLM’s understanding of geophysical signal patterns, noise discrimination, and time-series data analysis.
 - **Earthquake magnitude estimation:** Determine the earthquake magnitude based on the seismic amplitude at the location of the S-wave seismic phase.
 - **Earthquake source-receiver distance inference:** Single-station earthquake location is simplified to determining the distance from the earthquake hypocenter to the geophone through the distance between the P-wave and S-wave seismic phases.
- L2-Geophysics imaging:
 - **Salt body detection:** Identifying subsurface salt dome structures in geological or seismic data, testing the LLM’s domain knowledge in geophysics, spatial pattern recognition, and geological feature interpretation.
 - **salt body location:** Precisely determining the spatial coordinates or depth of salt bodies within geological formations, evaluating the LLM’s capability in spatial reasoning, multi-dimensional data integration, and quantitative analysis accuracy.

A.2.6 Oceansphere

We build a multi-layer MLLM benchmark for the oceansphere based primarily on satellite and analysis data products, featuring **8 practical L4 subtasks**. This domain includes three representative L2 scenarios: *Marine Oil Spills and Debris Monitoring (L2)*, *Extreme Oceanic Events Warning (L2)*, and *Ocean Phenomena Detection (L2)*. The Marine Oil Spills and Debris Monitoring [1] scenario uses multi-source remote sensing and in situ water quality data to track the spatial distribution and temporal dynamics of oil contamination and floating debris, supporting environmental management and emergency response. The Extreme Oceanic Events Warning [26, 48] scenario targets the detection and prediction of major climate modes such as El Niño–Southern Oscillation (ENSO) and the Indian Ocean Dipole (IOD), aiming to mitigate their societal and economic impacts. The Ocean Phenomena Detection scenario [17, 38] involves identifying ocean features like eddies and marine fog, which are key for maritime safety and ecological studies.

- L2-Extreme Events:
 - **Enso identification:** Critical for mitigating global climate extremes, this task classifies ENSO events (e.g., El Niño and La Niña) by analyzing the Pacific SST anomaly maps.
 - **Iod identification:** Essential for monsoon forecasting and reducing compound risks in Indian Ocean nations, this task identifies Indian Ocean Dipole phases (positive/negative) from SST anomalies, similar to ENSO identification.
 - **Enso forecast:** As a complement to ENSO identification, this task predicts whether or what type of ENSO event will occur several months ahead using global SST anomaly maps of the past six months, which requires the model to capture the temporal evolution process.
 - **Iod forecast:** As a complement to IOD identification, this task predicts IOD event occurrence and type, similar to ENSO forecasting.
- L2-Phenomenon Detection:
 - **Eddy identification:** Fundamental for marine ecosystem management, this task identifies eddy types (cyclonic/anticyclonic) from the chlorophyll grayscale satellite image.

- **Marine fog detection:** Critical for maritime safety and intelligent navigation, this task identifies fog presence via satellite imagery.
- **Eddy Localization :** As a complement to eddy localization, this task detects the location of eddies, enhancing search-and-rescue operations and pollution mitigation.
- L2-Marine Debris and Oil Pollution:
 - **Marine Pollution Type Classification:** Marine Pollution Type Classification refers to the scientific method of systematically categorizing marine pollutants based on their sources or characteristics (e.g., oil spills, plastic waste, chemical discharges)," which can test an LLM's domain knowledge in environmental science, multi-category semantic comprehension, and fine-grained classification capabilities.

A.2.7 Cryosphere

We conduct an MLLM benchmark for the cryosphere primarily based on sea ice reanalysis data, glacial imagery, and graphical plots, incorporating **8 practical L4 subtasks**. We identify two representative L2 scenarios within the cryosphere: *Sea Ice Forecasting (L2)* and *Glacier Analysis (L2)*. Sea ice forecasting focuses on predicting the dynamic changes of sea ice in polar regions. Arctic sea ice is crucial for understanding global climate change [7, 103]. Its continuous decline over the last few decades has made sea ice forecasting significant for navigating through the Arctic Ocean during melting seasons. Moreover, the loss of the Antarctic sea ice would greatly impact the global sea level. Glacier analysis [35, 11], aims to study the glacial movements and changes of glaciers over time. The complete task details are as follows.

- L2-Glacier analysis:
 - **Glacial Lake Recognition:** A melting glacier could result in multiple glacial lakes. Identifying them could provide valuable information for analyzing the variation trend of glaciers. We provide the model with images of glacial lakes, glaciers, and regular lakes. The model is asked to output the quantity of glacial lakes. This L4 task not only assesses the model's ability to identify glacial lakes from the others, it also assesses whether the model is capable of accurately reasoning about the overall quantities.
 - **Glacier Melting Estimation:** To evaluate the model's ability to analyze glacier data, we first present the model with the observation of glacier melting rate data and a sample chart showing the correlation between the melting rate and displayed color. Then, we provide two predictive charts from different models, and the model is required to identify which one better matches the provided real-world observation. Additionally, we show the model images of different glaciers at various times to see if it can determine which glacier is more likely to be in a melting state.
 - **Slide Recognition:** This task is designed to assess the model's ability to determine glacier landslide risks. First, we show it images of different glaciers and ask it to judge which one is more likely to experience a landslide based on their melting conditions. Then, we provide traverse and longitudinal melting profiles showing the melting rates and thickness of glaciers at different locations in Greenland, and ask the model to determine which glacier is more prone to landslides.
- L2-Sea ice forecast:
 - **SIC Estimate SIT:** To further test the model's ability to analyze sea ice concentration data, we provide it with a sea ice thickness variation trend chart, and sea ice concentration data from a date following the last point on that chart. The model is instructed to forecast the sea ice thickness of the following day based on inputs.
 - **SIC Estimate SIV:** To explore the model's ability to analyze sea ice concentration data, we provide it with a sea ice volume variation trend chart, and sea ice concentration data from a date following the last point on that chart. We then assess whether the model can accurately forecast the sea ice volume for the following day based on those two inputs.
 - **SIT Trend Prediction:** In this L4 task, we further evaluate the model's ability to directly analyze the trend data and make reasonable forecasts. Similarly, we provide the model with the previous year's sea ice thickness variation curve and the trend up to a certain point in the following year. Then, the model is required to predict subsequent sea ice thickness according to input data.

- **SIV Trend Prediction:** In this L4 task, we provide the model with the previous year's sea ice volume variation curve and the trend up to a certain point in the following year, to test the model's ability to make short-term forecasts of sea ice volume based on given data.
- **Sea Ice Extent Estimation:** Questions in this L4 task are designed to assess the model's ability to distinguish between Antarctic and Arctic sea ice, determine the melting season, i.e., evaluate the sea ice extent changes over time, and estimate the sea ice extent area from a given sea ice concentration map.

Table 8: **Characteristics of each task (L4 dimension) in human-activity sphere, Biosphere, Cross-sphere and Lithosphere.** Human-activity sphere has 27 subtasks, Biosphere has 15 subtasks, Cross-sphere has 7 subtasks, Lithosphere has 8 subtasks.

L1	L2	L3	L4 Task Description	Format	Samples	Answer Type
Human-activity sphere	Surface Disaster	Perception	Change detection counting of post-disaster completely destroyed building	VQA	502	Multiple Choice/Open-ended
			Counting of post-disaster partially damaged building	VQA	498	Multiple Choice/Open-ended
			Landslide events caption	Images Caption	4	Caption
		General Reasoning	Building damage prediction	VQA	499	Multiple Choice/Open-ended
			Disaster prediction	VQA	500	Multiple Choice/Open-ended
			Disaster type classification	VQA	500	Multiple Choice/Open-ended
			Geolocation estimation of disaster-affected regions from imagery	VQA	502	Multiple Choice/Open-ended
			Individual building damage assessment	VQA	107	Multiple Choice/Open-ended
			Multi-image individual visual localization task	VQA	102	Multiple Choice/Open-ended
			Spatial relationships under complex conditions	VQA	99	Multiple Choice/Open-ended
		Visual grounding of damaged individual buildings	VQA	102	Multiple Choice/Open-ended	
		CoT	Individual building damage assessment	VQA/CoT	107	Multiple Choice/Open-ended
			Multi-image individual visual localization task	VQA/CoT	102	Multiple Choice/Open-ended
			Spatial relationships under complex conditions	VQA/CoT	99	Multiple Choice/Open-ended
			Visual grounding of damaged individual buildings	VQA/CoT	102	Multiple Choice/Open-ended
	Urban Development	Perception	Fine-grained object recognition	VQA	514	Multiple Choice/Open-ended
			Overall counting	VQA	502	Multiple Choice/Open-ended
		General Reasoning	Counting under complex conditions	VQA	754	Multiple Choice/Open-ended
			Individual building height estimation	VQA	101	Multiple Choice/Open-ended
			Overall building height estimation	VQA	100	Multiple Choice/Open-ended
		CoT	Individual building height estimation	VQA/CoT	101	Multiple Choice/Open-ended
	Overall building height estimation		VQA/CoT	100	Multiple Choice/Open-ended	
	Land Use	Perception	Overall land type classification	VQA	509	Multiple Choice/Open-ended
			Fine-grained land type classification	VQA	509	Multiple Choice/Open-ended
			Visual grounding of land types	Visual Grounding	508	Bounding Box
			Visual localization of land use types	VQA	509	Multiple Choice/Open-ended
		General Reasoning	Complex land counting	VQA	449	Multiple Choice/Open-ended
Biosphere	Crop growth monitoring	Perception	Dead oil palm counting	VQA	828	Multiple Choice/Open-ended
			Dead oil palm identification	VQA	828	Multiple Choice/Open-ended
	Environmental pollution monitoring	Perception	Terrestrial oil spill area calculation	VQA	123	Multiple Choice/Open-ended
			Terrestrial oil spill counting	VQA	123	Multiple Choice/Open-ended
	Human footprint assessment	Scientific-Knowledge Reasoning	Human footprint assessment	VQA	300	Multiple Choice/Open-ended
			Human footprint index estimation	VQA	300	Multiple Choice/Open-ended
	Species Distribution Prediction	Perception	Tree species prediction	VQA	500	Multiple Choice/Open-ended
			Tree species proportion prediction	VQA	500	Multiple Choice/Open-ended
		Expert- knowledge Deductive Reasoning	Animal classification	VQA	108	Multiple Choice/Open-ended
			Geographical location inference of plant species	VQA	500	Multiple Choice/Open-ended
Global animal counting			VQA	110	Multiple Choice/Open-ended	
Species distribution prediction	VQA	1000	Multiple Choice/Open-ended			
Vegetation monitoring	Scientific-Knowledge Reasoning	Fractional vegetation cover estimation	VQA	300	Multiple Choice/Open-ended	
		Leaf area index estimation	VQA	300	Multiple Choice/Open-ended	
		Peak vegetation coverage area grounding	VQA	300	Multiple Choice/Open-ended	
Cross-sphere	Bird species prediction	Scientific-Knowledge Reasoning	Most likely species to occur	VQA	900	Multiple Choice/Open-ended
			Species occurrence probability estimation	VQA	453	Multiple Choice/Open-ended
			Species richness estimation	VQA	900	Multiple Choice/Open-ended
	Carbon flux monitoring	Scientific-Knowledge Reasoning	Carbon flux estimation	VQA	330	Multiple Choice/Open-ended
Global Flood Forecasting	Scientific-Knowledge Reasoning	Flood detecting	VQA	596	Multiple Choice/Open-ended	
		Flood predicting	VQA	277	Multiple Choice/Open-ended	
		Flood events caption	Images Caption	28	Caption	
Lithosphere	Earthquake monitoring and prediction	Perception	P-wave phase picking	VQA	300	Multiple Choice/Open-ended
			S-wave phase picking	VQA	300	Multiple Choice/Open-ended
			Earthquake or noise classification	VQA	300	Multiple Choice/Open-ended
	Scientific-Knowledge Reasoning	Earthquake magnitude estimation	VQA	300	Multiple Choice/Open-ended	
		Earthquake source-receiver distance inference	VQA	300	Multiple Choice/Open-ended	
	Geophysics imaging	Perception	Salt body location	Visual Grounding	302	Bounding Box
Salt body detection			VQA	329	Multiple Choice/Open-ended	
Volcanic activity	Perception	Volcanic activity caption	Images Caption	2	Caption	

Table 9: **Characteristics of each task (L4 dimension) in Atmosphere, Oceansphere and Cryosphere.** Atmosphere has 36 subtasks, Oceansphere has 8 subtasks, Cryosphere has 8 subtasks.

L1	L2	L3	L4 Task Description	Format	Samples	Answer Type		
Atmosphere	Interannual climate variation	Perception	ENSO feature analysis	VQA	86	Multiple Choice/Open-ended		
			Long-term Precipitation trend analysis	VQA	50	Multiple Choice/Open-ended		
			Long-term Temperature trend identification	VQA	51	Multiple Choice/Open-ended		
	Medium-term weather events	Perception	Cyclone movement identification	VQA	185	Multiple Choice/Open-ended		
			Cyclone phase identification	VQA	90	Multiple Choice/Open-ended		
			C-WAVE Caption	Images Caption	17	Caption		
			Event localization	VQA	93	Multiple Choice/Open-ended		
			Event intensity identification	VQA	594	Multiple Choice/Open-ended		
			Event onset identification	VQA	42	Multiple Choice/Open-ended		
			Event trend analysis	VQA	575	Multiple Choice/Open-ended		
			H-WAVE Caption	Images Caption	17	Caption		
			Geopotential pattern identification	VQA	33	Multiple Choice/Open-ended		
			Moisture flux analysis	VQA	150	Multiple Choice/Open-ended		
			System identification	VQA	231	Multiple Choice/Open-ended		
	Scientific-Knowledge Reasoning	Scientific-Knowledge Reasoning	Storm Caption	Images Caption	8	Caption		
			System evolution trend analysis	VQA	91	Multiple Choice/Open-ended		
	SEVIR Weather	Scientific-Knowledge Reasoning	Event type prediction	VQA	300	Multiple Choice/Open-ended		
			Miss alarm estimation	VQA	300	Multiple Choice/Open-ended		
			Movement prediction	VQA	200	Multiple Choice/Open-ended		
			Rotate center prediction	VQA	93	Multiple Choice/Open-ended		
Seasonal weather events	Perception	Precipitation anomaly identification	VQA	75	Multiple Choice/Open-ended			
		Seasonal comparison	VQA	101	Multiple Choice/Open-ended			
		Temperature anomaly identification	VQA	75	Multiple Choice/Open-ended			
Short-term weather events	Perception	Event intensity identification	VQA	323	Multiple Choice/Open-ended			
		Event localization	VQA	133	Multiple Choice/Open-ended			
		Event trend analysis	VQA	297	Multiple Choice/Open-ended			
	Scientific-Knowledge Reasoning	Scientific-Knowledge Reasoning	Event type identification	VQA	139	Multiple Choice/Open-ended		
			Dynamic feature identification	VQA	40	Multiple Choice/Open-ended		
			Event evolution analysis	VQA	90	Multiple Choice/Open-ended		
Typhoon	Scientific-Knowledge Reasoning	Thermodynamic feature identification	VQA	40	Multiple Choice/Open-ended			
		Pressure estimation	VQA	847	Multiple Choice/Open-ended			
		Radius of major gale axis estimation	VQA	847	Multiple Choice/Open-ended			
		Radius of minor gale axis estimation	VQA	847	Multiple Choice/Open-ended			
		Radius of major storm axis estimation	VQA	847	Multiple Choice/Open-ended			
		Radius of minor storm axis estimation	VQA	847	Multiple Choice/Open-ended			
Cryosphere	Glacier analysis	Perception	Wind estimation	VQA	847	Multiple Choice/Open-ended		
			Glacial Lake Recognition	VQA	12	Multiple Choice/Open-ended		
	Sea ice forecast	Scientific-Knowledge Reasoning	Scientific-Knowledge Reasoning	Glacier Melting Estimation	VQA	10	Multiple Choice/Open-ended	
				Slide Recognition	VQA	8	Multiple Choice/Open-ended	
				SIC Estimate SIT	VQA	20	Multiple Choice/Open-ended	
				SIC Estimate SIV	VQA	20	Multiple Choice/Open-ended	
Oceansphere	Extreme Events	Perception	SIT Trend Prediction	VQA	30	Multiple Choice/Open-ended		
			SIV Trend Prediction	VQA	30	Multiple Choice/Open-ended		
		Scientific-Knowledge Reasoning	Scientific-Knowledge Reasoning	Sea Ice Extent Estimation	VQA	100	Multiple Choice/Open-ended	
				Enso identification	VQA	146	Multiple Choice/Open-ended	
	Marine Debris and Oil Pollution	Perception	Perception	Iod identification	VQA	140	Multiple Choice/Open-ended	
				Enso forecast	VQA	152	Multiple Choice/Open-ended	
		Phenomenon Detection	Perception	Perception	Iod forecast	VQA	145	Multiple Choice/Open-ended
					Marine Pollution Type Classification	VQA	110	Multiple Choice/Open-ended
Phenomenon Detection	Perception	Perception	Eddy identification	VQA	204	Multiple Choice/Open-ended		
			Marine fog detection	VQA	200	Multiple Choice/Open-ended		
Phenomenon Detection	Perception	Perception	Eddy identification	Visual Grounding	166	Multiple Choice/Open-ended		
			Eddy Localization	Visual Grounding	166	Multiple Choice/Open-ended		

A.3 Data Processing Strategies for the Six Spheres.

A key point of inquiry is how Multimodal Large Models (MLLMs) process or adapt to the full range of input modalities provided in our dataset. This section elaborates on the data processing strategies employed for the 33 diverse sources integrated into OmniEarth-Bench.

Our general workflow involves domain experts collaborating with annotators to manually transform raw inputs into formats suitable for MLLMs, such as RGB images paired with questions. The specific approach depends on the nature of the original data:

- **When RGB images are available:** Experts select scientifically relevant images for Visual Question Answering (VQA) tasks and design corresponding questions, with annotators assisting in formulating the responses and distractors.
- **When only raw data is provided:** Experts visualize key variables as RGB images based on predefined dimensions and scientific conventions. Some detailed examples using meteorological data are included below.

The complete processing code and pipeline documentation will be released on our project website in a future update for community use. The following provides a detailed breakdown for several of the Earth’s spheres.

Cryosphere To create a test-ready QA benchmark for Level-4 sea-ice analytics—covering Sea-Ice Extent (SIE) estimation, Sea-Ice Volume (SIV) trend prediction, SIV-from-SIC estimation, Sea-Ice Thickness (SIT) trend prediction, and SIT-from-SIC estimation—we (1) acquire daily sea-ice concentration fields from NSIDC’s G02202-v4 archive and Arctic SIV time-series from PIOMAS, (2) decode the NetCDF products with the open-source `netCDF4` package, (3) derive daily SIE and basin-averaged SIC, (4) plot SIE, SIC, and SIV evolutions as authoritative references, and (5) assemble question–answer pairs that juxtapose data-driven ground-truth with intentionally misleading distractors. Each question is purpose-built to probe a specific facet of sea-ice reasoning in multimodal large-language models.

Biosphere For multi-scenario ecological Q&A tasks, we built a high-resolution dataset combining remote sensing imagery, eco-meteorological data, and multi-source annotations. It includes MODIS 7-band, Landsat, and UAV images; COCO-format dead oil palm labels; multi-band oil spill masks; surface vegetation and human footprint indices; daily meteorological sequences (temperature, humidity, radiation, wind, precipitation); 19 SatBird bioclimatic variables; carbon flux (NEE) observations; and structured metadata (CSV/JSON with means, species probabilities, and patch IDs). Preprocessing involved three main stages:

1. Metric Computation and Normalization

- **GLASS:** Mean FVC \times 0.004 and LAI \times 0.1 values written to CSV.
- **HFP:** Aggregated raster means.
- **CarbonSense:** Removed missing rows, converted meteorological variables to text, and aligned them with MODIS images.
- **SatBird:** Stratified by species richness and extracted species probabilities from hotspot JSON.
- **ROSID:** Binarized masks, counted connected domains, and calculated oil spill area from pixel count.
- **MOPAD:** Filtered `category_id == 1` to count dead oil palms.

2. Image Standardization

- Converted SatBird `.tif` to `.jpg`, CarbonSense `.pk1` to `.png`.
- Linked GLASS/HFP patches to full 7-band MODIS imagery.
- Preserved original resolution for UAV and Landsat images.

3. Thresholding and Answer Binning

- Mapped continuous variables (FVC, LAI, HFP) to preset intervals.
- Generated distractors using ± 20 –40% (ROSID) or ± 2 –10 trees (MOPAD) around ground truth.
- Binned species occurrence probabilities into [0, 0.3], [0.3, 0.6], and [0.6, 1].
- Converted oil spill pixel count \times 900 m² to km² and rounded.

Atmosphere For atmospheric weather events, we primarily use reanalysis datasets such as ERA5, with meteorological variables visualized as RGB images that include variable names, legends, latitude-longitude grids, and national boundaries.

1. **Short- and Medium-Term Events:** We compiled global event records from 1979–2020, retrieved corresponding timestamps from ERA5, and used 1-hour and 6-hour intervals for short- and medium-term events, respectively. For multivariable or long-duration cases, the interval was increased fourfold to limit image volume.
2. **Seasonal and Interannual Events:** These longer-range events require post-processing of raw model data. We use NOAA’s Global Reports (2010.01–2025.03) featuring visualized anomalies and regional summaries. Following LLaVA’s methodology, we use ChatGPT-4o to generate QA pairs. Seasonal inputs include all 12 monthly reports from a given year; interannual tasks use annual reports from 2010–2024.

Lithosphere For seismic waveform analysis, we leverage the large-scale Stanford Earthquake Dataset (STEAD). The process involves several key stages: (1) we select high-quality, three-component seismic waveforms and filter out samples with missing components or low signal-to-noise ratios; (2) all waveforms are standardized to a uniform 100 Hz sampling rate, normalized, and formatted into 60-second slices; and (3) these raw waveforms are converted into standardized RGB image representations for visual analysis. Based on these images, we construct VQA tasks covering five core seismic challenges: earthquake/noise classification, P-wave and S-wave arrival picking, epicentral distance inference, and magnitude estimation. For each task, the ground-truth answer (True Value) is derived from STEAD’s expert-annotated labels, while distractor answers (False Values) are systematically generated by applying controlled perturbations to the true values to test model robustness.

Oceansphere For the oceansphere, our data processing varies based on the source format. For analyzing climate phenomena like the El Niño-Southern Oscillation (ENSO), we use the ERSSTv5 Sea Surface Temperature (SST) dataset. The VQA construction involves: (1) calculating 30-year centered climatology and 3-month averaged anomalies; (2) computing the Niño3.4 index to classify ENSO events; (3) visualizing the SST anomalies as RGB maps; and (4) selecting relevant maps to construct question-answer pairs. This supports two primary tasks: identifying the current ENSO state using Pacific anomaly maps from the peak DJF season, and forecasting future ENSO events using a sequence of six consecutive global anomaly maps as input. For datasets that are already in visible light RGB format, such as the MADOS dataset for marine pollution monitoring from Sentinel-2 imagery, the process is more direct. It primarily involves selecting scientifically relevant images and constructing VQA tasks around visually identifiable features, such as classifying pollution types (e.g., oil spills, marine debris, floating algae) and visually localizing targets like oil platforms or specific patches of contamination.

Human-activity sphere For the human-activity sphere, the data is predominantly in visible light RGB format, simplifying the preprocessing pipeline. We utilize a range of specialized datasets such as xView2, UBCv1, and WHU-OHS to construct VQA tasks focused on disaster impact assessment and fine-grained urban and land-use analysis. These tasks include identifying disaster types (e.g., floods, wildfires), counting damaged or destroyed buildings by comparing pre- and post-event imagery, assessing the damage level of individual structures, and performing fine-grained urban analysis, such as object counting (vehicles, buildings), land-use classification (farmland, urban built-up), and visual localization of specific man-made features.

A.4 Construction Details of Different Question Formats.

A.4.1 Chain-of-Thought (CoT) Annotation Details.

This section provides a detailed account of the motivation, scope, and rigorous workflow used to construct the Chain-of-Thought (CoT) annotations for the Level-4 (L4) evaluation tasks in OmniEarth-Bench.

Motivation and Scope During the developmental phase of our benchmark, we identified a subset of tasks that were exceptionally challenging for current Multimodal Large Models (MLLMs). These tasks, such as the visual localization of a single damaged building across pre- and post-disaster imagery, could not be solved through single-step perception or retrieval. They inherently require a complex, multi-step reasoning process that involves identifying context, comparing features, eliminating distractors, and finally pinpointing the target.

Therefore, the primary motivation for introducing CoT annotations was to create a mechanism to explicitly evaluate the capacity of MLLMs to perform and follow logical, multi-step scientific reasoning. These annotations are designed as a gold standard for evaluation, not for model training.

This annotation effort was strategically focused on 6 of our most demanding sub-tasks, where such complex reasoning is indispensable. In total, this resulted in a collection of 610 samples meticulously annotated with detailed reasoning chains.

Annotation Paradigm and Workflow To ensure the quality, objectivity, and logical consistency of our CoT annotations, we designed and implemented a rigorous, multi-stage, human-in-the-loop workflow. This process was structured to leverage the capabilities of advanced AI while relying on human expertise for creation and final validation. The workflow is detailed below:

1. **AI-Generated Reference Chain.** For each question, a high-quality reference reasoning chain was first generated using the GPT-4o model. Crucially, to ensure the reference was accurate and complete, the model was provided with both the question and the ground-truth answer. This initial chain served as a comprehensive, machine-generated example of a possible logical pathway.
2. **Human-Authored Key Steps.** Certified annotators, all holding at least a bachelor’s degree, were then tasked with creating a new and independent set of crucial reasoning steps based on their own analysis of the problem, using the AI-generated chain only as a reference.
3. **Ensuring Logical Independence and Diversity.** To prevent mere paraphrasing of the AI’s output and to encourage diverse, human-centric logic, a strict quality constraint was enforced: the semantic and logical overlap between the final human-authored steps and the initial AI-generated reference chain had to be less than 20%. This ensured that our CoT annotations represent genuine human reasoning patterns.
4. **Domain Expert Verification.** The newly created CoT annotations were subsequently passed to our team of domain experts (Ph.D. students in relevant Earth science fields) for a final round of verification. They meticulously checked each reasoning chain for:
 - *Logical Soundness:* Ensuring the steps flow logically from one to the next.
 - *Scientific Accuracy:* Validating any domain-specific knowledge or claims.
 - *Completeness:* Confirming that all necessary steps to reach the correct conclusion are present.
5. **Refinement and Condensation.** Lastly, all expert-validated steps were refined to be as concise as possible. This involved removing redundant phrases and retaining only the core logic and essential visual or data-driven cues. The goal was to produce an information-dense yet easy-to-follow reasoning pathway that represents the most efficient and accurate thought process to solve the task.

This structured paradigm guarantees that our CoT annotations are not only correct and logical but also a robust and reliable tool for evaluating the sophisticated reasoning capabilities of advanced AI models in the Earth sciences.

A.4.2 Open-Ended Questions Annotation Details.

Motivation and Scope To more rigorously assess the true generative and reasoning capabilities of Multimodal Large Language Models (MLLMs), we introduced an open-ended question format for

the OmniEarth-Bench. The standard Multiple-Choice Question (MCQ) format, while efficient for broad-scale evaluation, provides explicit options that can act as "scaffolds" or hints for the model. This mitigates the risk of models guessing the correct answer from a limited set of choices without genuine understanding. The open-ended format removes these scaffolds, compelling the model to generate answers from scratch and providing a more challenging and realistic measure of its knowledge and reasoning abilities in the Earth science domain.

The open-ended questions in OmniEarth-Bench are systematically transformed from the existing L4 subtasks originally designed in the MCQ format. This transformation process is not uniform but is instead tailored to the intrinsic nature of the answer for each task. We categorized all L4 subtasks into four distinct types to guide this conversion:

1. **Classification with a small, fixed label set:** Tasks where the answer is one of a few predefined categories (e.g., ENSO phases).
2. **Classification with a large label set:** Tasks where the answer is a choice from a larger, but still finite, set of options (e.g., direction of cyclone movement).
3. **Exact regression:** Tasks that require a precise numerical answer (e.g., counting objects).
4. **Interval regression:** Tasks where the answer is a numerical or temporal range (e.g., duration of an event).

Workflow The construction and validation of open-ended question-answer pairs followed a meticulous, expert-driven workflow:

1. **Task Classification:** Domain experts first categorized each of the 103 L4 subtasks into one of the four types defined in the Scope. This initial step determined the specific transformation strategy to be applied.
2. **Prompt Transformation:** Based on its category, the prompt for each task was re-engineered:
 - For tasks with **small, fixed label sets**, the multiple-choice options were removed, and the question was rephrased to directly ask for the answer (e.g., "What is the ENSO phase shown in the image?").
 - For tasks with **large label sets**, the candidate labels were explicitly listed within the prompt itself, instructing the model to choose and generate the answer from the provided list (e.g., "From the following list [North, Northeast, East...], what is the direction of movement...?").
 - For **exact regression** tasks, the question was rephrased to directly ask for the numerical value (e.g., "How many deceased oil palm trees are in the image?").
 - For **interval regression** tasks, the prompt was modified to specify the required answer format (e.g., "Provide the time range in the format 'Start Month - End Month'.").
3. **Golden Answer Formulation:** The correct option from the original MCQ (e.g., option 'C') was converted into its full-text or numerical "golden answer" (e.g., the text "Strong El Niño" or the number "15").
4. **Expert Review and Refinement:** Finally, all newly generated open-ended questions and their corresponding golden answers were rigorously reviewed by the domain experts. This step ensured that the rephrased questions were unambiguous, scientifically accurate, and that the golden answers remained correct and appropriately formatted.

Evaluation Method The evaluation of open-ended questions poses a unique challenge, as traditional exact string matching is often too rigid to account for semantically correct but varied natural language responses. Therefore, we employ a **Large Language Model (LLM) as an automated judge** for assessing the correctness of generated answers. Specifically, a powerful, state-of-the-art LLM (e.g., GPT-4o) is provided with the original question, the MLLM's generated answer, and the expert-defined golden answer. The LLM's task is to determine whether the MLLM's answer is semantically equivalent to or sufficiently captures the essence of the golden answer, thereby marking it as correct or incorrect. This approach leverages the advanced semantic understanding capabilities of LLMs to provide a more nuanced and fair assessment of open-ended generative performance, overcoming the limitations of keyword-based or fixed-choice evaluations.

A.4.3 Images Caption Annotation Details.

Motivation and Scope Standard image captioning benchmarks typically focus on describing the literal content of an image, which is insufficient for the complex analytical needs of Earth science. In this domain, a deep understanding requires not only recognizing visual patterns in satellite imagery but also integrating them with external, contextual scientific data. To address this gap, we designed a specialized captioning task for OmniEarth-Bench. The motivation is twofold: first, to create a benchmark that evaluates an MLLM’s ability to perform **multimodal fusion**, synthesizing information from both visual satellite data and textual historical disaster data; second, to test a model’s capacity for domain-specific reasoning by requiring it to act as a meteorological expert, thereby moving beyond simple object description to nuanced scientific interpretation.

The scope of this task is centered on significant climate-related disasters, leveraging a combination of satellite and historical data sources.

1. **Image Data Source:** The visual data consists of multispectral images from the **Microwave Humidity Sounder (MHS)** satellite. Each event is represented by a set of images corresponding to MHS’s five distinct spectral bands, capturing 12 hours of observational data.
2. **Contextual Data Source:** The textual data is sourced from the **EM-DAT International Disaster Database**, which provides detailed historical records of climate events.
3. **Event Types:** The task covers a range of severe weather and climate phenomena, including **storms, floods, landslides, wildfires, cold waves, and heat waves**.
4. **Output:** The deliverable is a collection of image sets paired with single-paragraph, detailed captions. Each caption cohesively integrates the visual evidence from the MHS imagery with the factual context from the corresponding EM-DAT record.

Workflow The creation of the image-caption pairs followed a systematic, multi-stage workflow, ensuring both scientific rigor and data quality.

1. **Raw Data Acquisition and Preprocessing:**
 - Level 1B data from the MHS satellite, which is initially sparse and irregular, was collected.
 - This raw data was processed using a **remapping algorithm** to project the sparse observation points onto a regular, spatially coherent global grid, creating a dense image-like representation for each spectral channel.
2. **Event Identification and Cropping:**
 - Using the EM-DAT database, significant historical climate disasters were identified, and their specific geographic locations and timelines were extracted.
 - An **event cropping algorithm** was then applied to the global satellite data grids. For each identified disaster, the corresponding 12-hour, 5-channel image sequence was precisely cropped from the global map based on the event’s location and time.
3. **Automated Caption Generation with Multimodal Input:**
 - The cropped set of multispectral satellite images and the associated textual disaster report from EM-DAT were provided as combined input to a state-of-the-art LLM (GPT-4o).
 - A specialized prompt was engineered to instruct the model to act as a "meteorological analysis expert." The prompt explicitly required the model to generate a single, cohesive paragraph that analyzes and describes the event by synthesizing relevant details from *both* the images and the historical data.
4. **Expert Review and Validation:**
 - Finally, every automatically generated caption underwent a rigorous review by human domain experts. This validation step was crucial for verifying the scientific accuracy of the interpretation, the factual correctness of the fused information, and the overall linguistic quality and coherence of the caption. Any captions that were inaccurate or failed to properly integrate the data sources were either refined by experts or discarded to maintain the high standard of the benchmark.

A.5 Detailed results of specific sub-tasks (L-4 dimension).

Worse performance of Qwen2.5-VL. Qwen2.5-VL lagged behind contemporary open-source models like InterVL3 on Earth-related tasks, with both its 7B and 72B versions rarely ranking first in any L4 subtask. Despite its larger parameter size, the 72B model often scored zero on multiple tasks. However, this low accuracy shouldn’t be seen as a lack of capability. Qwen2.5-VL often responds with “E (unable to answer)” when lacking domain knowledge—an honest approach. In contrast, some models tend to guess when uncertain, which is less desirable.

Many models scored zero on various sub-tasks. Even the top-performing InternVL3-78B failed on several. GPT-4o, a widely used closed-source model, recorded zero accuracy on nearly half the tasks. These results underscore the effectiveness and domain specificity of our sub-task design.

No significant gap between closed-source and open-source models. Although Gemini and Claude3 slightly lag behind LLaVA-OneVision and InternVL3 on sub-tasks, the gap is minimal. This indicates that open-source multimodal models are still well-suited for advancing Earth science research and agent development, without relying exclusively on closed-source alternatives.

Poor performance of some subtasks in Cross-sphere. In the cross-sphere species richness prediction task, no model surpassed 10% accuracy on 900 test samples, which aligns with expectations given the task’s complexity. Integrating climate variables, satellite imagery, and vegetation factors creates a highly intricate prediction challenge beyond the capabilities of current models.

Table 10: CoT performance of each L4 subtasks. We mark the highest score of each metric in red, and second highest underlined.

Task	Num.	Qwen2.5-VL-7B			LLaVA-OneVision-7b			InternVL3-8B			InternVL3-78B		
		Precision	Recall	F1	Precision	Recall	F1	Precision	Recall	F1	Precision	Recall	F1
Multi-image Visual Localization	102	95.87	31.21	47.09	93.28	40.36	56.34	93.89	41.34	<u>57.40</u>	97.49	43.74	60.39
Visual grounding of damaged individual buildings	102	95.97	25.98	40.89	92.38	22.92	36.73	95.86	33.47	<u>49.62</u>	91.99	42.58	58.21
Overall building height estimation	100	83.97	14.50	24.73	83.73	18.17	29.86	93.82	20.00	32.97	92.59	19.50	<u>32.22</u>
Spatial relationships under complex conditions	99	94.51	35.98	<u>52.12</u>	91.75	22.27	35.84	93.79	36.60	52.65	96.25	32.55	48.65
Individual building damage assessment	107	93.21	37.54	53.52	87.93	12.96	22.59	92.79	40.74	56.62	95.58	39.06	<u>55.46</u>
Individual building height estimation	101	92.49	12.71	22.34	87.69	13.2	22.95	91.77	13.37	<u>23.34</u>	90.46	14.36	24.78

InternVL3 outperforms other MLLMs in CoT tasks. The InterVL3 series performed strongly on CoT tasks, with both the 7B and 78B models achieving top results across all subtasks, showcasing their strength in geoscience chain-of-thought reasoning. Future geoscience reasoning tasks could benefit from further training and application of this series.

Table 11: Visual Grounding performance one each L4 subtasks.

L4	Num	Qwen2.5-VL-7B		LLaVA-OneVision-7b		InternVL3-8B		InternVL3-78B		GPT-4o		Gemini-2.0		Claude-3.7	
		acc@0.5	acc@0.7	acc@0.5	acc@0.7	acc@0.5	acc@0.7	acc@0.5	acc@0.7	acc@0.5	acc@0.7	acc@0.5	acc@0.7	acc@0.5	acc@0.7
Salt Body Location	302	0	0	5.3	0.33	8.94	1.66	4.3	0.33	0.08	0	0.13	0.04	0.02	0
Eddy Localization	166	3.01	0	1.81	0.6	6.63	0.6	13.86	3.61	0.12	0.01	0.34	0.06	0.2	0.07
Visual Grounding of Land Types	508	0.2	0.00	0.59	0.20	2.56	0.59	2.36	0.20	0.02	0.00	0.03	0.00	0.00	0.00

Visual grounding performance is notably poor across all models It exposes two main shortcomings: limited geoscientific knowledge and weak visual localization capabilities. Both open- and closed-source models fall short in these aspects.

Table 12: **VQA Performance in L4 dimension.** We mark the highest score of each metric in red, and second highest underlined.

Domain	L4-task	Num	Qwen2.5-VL		InternVL3		LLaVA-OV	GPT-4o	Gemini	Claude3
			7B	72B	8B	78B	7B			
Human-activity	Change detection...	502	6.97	1.39	43.03	72.51	<u>85.06</u>	0	74.1	10.36
	Partially damaged...	498	1.41	0	4.02	<u>45.98</u>	<u>50.6</u>	0	11.24	0.8
	Building damage...	499	0.2	4.81	5.81	7.62	<u>33.87</u>	0	<u>8.22</u>	4
	Disaster prediction	500	0.8	<u>5.6</u>	4	0.6	0.6	0	0.2	2.8
	Disaster type...	500	1	6.2	6.6	8.2	1.6	0.4	4.2	<u>11.2</u>
	Geolocation...	502	12.15	9.76	36.25	<u>44.82</u>	31.67	2.59	36.45	33.47
	Fine-grained object...	514	10.89	19.46	21.98	30.35	<u>48.05</u>	0	<u>47.67</u>	16
	Overall counting	502	1.99	2.59	18.13	17.13	<u>21.12</u>	0.2	<u>31.67</u>	0
	Counting complex...	754	0.4	0	<u>31.75</u>	<u>19.05</u>	18.25	0.27	9.28	0.93
	Overall land...	509	0	0.2	<u>1.96</u>	1.38	1.38	0	1.57	1.18
	Fine-grained land...	509	3.93	6.68	26.13	6.48	<u>39.88</u>	<u>39.29</u>	30.26	32
	Visual localization...	509	1.38	3.54	5.11	4.52	1.77	0.39	<u>6.68</u>	1.57
	Land types ...	449	3.12	3.34	<u>24.5</u>	<u>16.04</u>	14.7	0	5.35	0
	Individual building ...	107	0.93	7.48	28.97	24.3	<u>47.66</u>	0	35.51	14.02
	Multi individual ...	102	10.78	13.73	28.43	<u>53.92</u>	<u>67.65</u>	8.82	41.81	43.14
	Spatial relation ...	99	22.22	21.21	33.33	<u>36.36</u>	23.23	2.02	<u>39.39</u>	16.16
Visual grounding ...	102	35.29	37.25	52.94	52.94	<u>65.69</u>	28.43	<u>56.86</u>	37.25	
Overall height ...	509	0	0.2	<u>1.96</u>	1.38	1.38	0	<u>1.57</u>	1.18	
Individual height ...	101	0	0	<u>45.54</u>	0	38.61	0	0	0	
Biosphere	Dead oil .. counting	828	52.9	47.95	48.67	<u>73.67</u>	<u>73.67</u>	0	56.04	<u>60.51</u>
	oil ..identification	828	<u>85.51</u>	<u>70.65</u>	81.52	83.33	<u>85.63</u>	0	51.81	77.29
	oil spill area ...	123	0	0	<u>5.69</u>	<u>5.69</u>	0	0	0	0
	oil spill counting ...	123	0	0.81	41.46	<u>53.66</u>	22.76	0	7.32	0
	footprint assess ..	300	0.33	0.67	<u>36</u>	26.33	22.67	0.67	7.67	<u>26.67</u>
	footprint index ..	300	0	0	3.33	3.33	<u>23.33</u>	0	0	<u>20</u>
	species prediction ..	500	5	15.2	35.6	<u>46.4</u>	<u>46.8</u>	0.8	15.8	13.2
	species proportion..	500	0	0.2	<u>26.2</u>	1.8	18.4	0	5.2	2.4
	Animal classification	108	4.63	1.85	15.74	<u>27.78</u>	<u>43.52</u>	0	9.26	2.78
	Geographical ...	500	4.6	13.4	18.2	26	50	10.4	38.6	<u>75.8</u>
	Species distribution...	1000	2.1	68.6	73.3	78.1	40.1	16.8	<u>91.5</u>	<u>90.2</u>
	Fractional ...	300	0	0	13	25	<u>56</u>	0	3.67	46
	Leaf area index...	300	0	0	7.33	14	<u>50</u>	0	0	29.33
animal counting...	110	0	3.64	0	<u>6.36</u>	2.73	0.91	<u>7.27</u>	0	
Peak vegetation...	300	9	0.67	<u>25</u>	8.33	24	0	18.3	24	
Cross-sphere	Most likely species...	900	0.11	18.89	20.89	<u>40.67</u>	21.89	0.22	36.67	<u>59.22</u>
	Species occurrence...	453	2.65	4.64	<u>58.5</u>	13.69	8.17	0	3.31	29.8
	Species richness ...	900	0	0	<u>9</u>	0.33	<u>7.67</u>	0	0	0
	Carbon flux ..	330	11.52	0	<u>24.85</u>	0.61	<u>25.45</u>	0	0.61	0
	Flood detecting	596	44.8	0	<u>52.18</u>	51.51	<u>52.35</u>	0	28.52	51
Cryosphere	Flood predicting	277	0	0	<u>91.7</u>	8.3	0	0	32.49	44.04
	Glacial Lake ..	12	25	25	<u>75</u>	<u>75</u>	75	50	<u>66.67</u>	<u>66.67</u>
	Glacier Melting...	10	30	10	<u>40</u>	<u>50</u>	30	10	30	<u>40</u>
	Slide Recognition...	8	<u>65.5</u>	0	37.5	62.5	<u>62.5</u>	12.5	62.5	50
	SIC Estimate SIT	20	0	0	55	<u>100</u>	45	85	80	90
	SIC Estimate SIV	20	0	0	45	<u>80</u>	40	50	<u>70</u>	<u>80</u>
	SIT Trend Prediction	30	3.33	0	50	<u>90</u>	50	40	46.7	<u>60</u>
	SIV Trend Prediction	30	0	0	36.67	<u>80</u>	36.67	13.33	<u>53.33</u>	20
Sea Ice Extent...	100	19	12	55	<u>59</u>	32	39	<u>59</u>	29	
Lithosphere	P-wave phase picking	300	8	11.33	10.67	<u>16</u>	8	6	<u>22.33</u>	11
	S-wave phase picking	300	36.67	35.33	<u>61.67</u>	41	32	16.67	<u>49.33</u>	28.33
	Earthquake or noise ..	300	44.67	86.33	63	59.33	52.33	50	<u>93.33</u>	<u>95</u>
	magnitude estim...	300	1.33	0	<u>38.33</u>	0	<u>32.67</u>	0	26.67	1.67
	source-receiver ...	300	20.33	0.67	<u>35.33</u>	6.67	<u>33</u>	1.67	14	21.67
	Salt body detection	329	0.91	0.91	15.81	<u>17.33</u>	14.29	2.43	<u>27.96</u>	11.25

Table 13: **VQA Performance in L4 dimension.** We mark the highest score of each metric in red, and second highest underlined.

Sphere	L4-task	Num	Qwen2.5-VL		InternVL3		LLaVA-OV	GPT-4o	Gemini	Claude3
			7B	72B	8B	78B	7B			
Atmosphere	Cyclone move...	185	8.65	2.16	37.84	<u>47.03</u>	34.59	6.49	38.38	<u>44.32</u>
	Cyclone phase...	90	0	0	<u>48.89</u>	0	<u>25.56</u>	1.11	25.56	5.75
	Event intensity...	594	17.34	44.61	38.72	0	30.14	13.21	<u>53.62</u>	<u>33.28</u>
	Event localization	93	18.28	5.38	<u>46.24</u>	41.94	33.33	18.98	<u>51.82</u>	43.07
	Event onset...	42	0	0	26.19	0	<u>35.71</u>	16.67	30.95	<u>38.1</u>
	Event trend...	575	0.18	0	<u>48.52</u>	0	36.87	2.96	<u>39.82</u>	14.7
	Geopotential...	33	18.18	12.12	<u>18.18</u>	<u>15.15</u>	12.12	<u>18.18</u>	9.09	30.3
	Moisture flux...	150	0	0	<u>66.00</u>	0	<u>53.34</u>	0	0	6.12
	System...	231	4.33	17.75	33.77	0	22.94	18.18	40.69	<u>52</u>
	System evolution...	91	2.2	0	40.66	0	56.04	17.58	<u>57.14</u>	<u>70</u>
	Event intensity...	323	18.89	13.62	<u>50.77</u>	0	34.37	30.64	<u>59.54</u>	18.31
	Event localization	133	1.5	0.75	<u>47.37</u>	0	13.53	25.85	<u>50.68</u>	21.05
	Event trend...	297	3.03	0	31.65	0	<u>35.69</u>	4.71	<u>41.08</u>	19.57
	Event type...	139	23.74	17.27	<u>36.69</u>	0	25.9	23.74	<u>27.34</u>	0
	Dynamic feature...	40	<u>45</u>	<u>67.5</u>	<u>37.5</u>	0	2.5	15	27.5	30.77
	Event evolution...	90	0	0	<u>24.44</u>	0	2.22	0	21.11	8
	Thermodynamic...	40	0	0	15	0	0	7.5	<u>20</u>	<u>15.79</u>
	Pressure...	847	0	0	<u>0.83</u>	0	<u>30.34</u>	0	0	0
	Radius (gale)...	847	0	0	21.49	0.59	<u>24.91</u>	0	0	<u>35.42</u>
	Radius (storm)...	847	0	0	<u>23.02</u>	0.71	14.76	0	0	<u>47.23</u>
	minor gale ...	847	0	0	0	<u>5.79</u>	<u>15.47</u>	0	0	0
	minor storm ...	847	0	0	1.89	0	4.84	0	0	0
	Wind estimation	847	0	0	0	5.79	<u>30.46</u>	0	0	0
	Precipitation ...	75	0	1.33	21.33	<u>28</u>	<u>22.67</u>	6.67	<u>28</u>	16
	Seasonal ...	101	8.91	9.9	<u>46.53</u>	0	<u>45.54</u>	27.52	40.5	40
	Temperature ...	75	16	18.67	45.33	<u>57.33</u>	48	29.33	<u>49.33</u>	48
	ENSO feature...	86	41.86	63.95	75.58	0	<u>77.91</u>	<u>90.7</u>	75.58	73.26
	Long.. Precipitation	50	0	0	<u>34</u>	<u>48</u>	26	20	26	32
	Long.. Temperature	51	0	0	<u>49.02</u>	<u>60.78</u>	27.45	39.22	25.49	27.45
	Event type ..	300	15	0	36	19	<u>42.67</u>	<u>20.67</u>	1	16
Miss alarm ..	300	0	0	19	<u>22</u>	<u>32</u>	0	0.67	8.33	
Movement ..	200	45	21	<u>76.5</u>	60.5	<u>81</u>	2	69	64.5	
Rotate center...	93	3.23	2.15	<u>62.37</u>	<u>75.27</u>	46.24	0	6.45	58.06	
Oceansphere	ENSO ..	146	21.92	<u>34.93</u>	33.56	17.81	23.97	31.51	26.03	<u>51.37</u>
	IOD Identification	140	4.29	<u>19.29</u>	12.86	4.29	12.14	<u>50</u>	5.71	12.86
	ENSO Forecast	152	0	3.29	23.03	<u>36.18</u>	15.79	6.58	<u>23.03</u>	19.74
	IOD Forecast	145	0	0	4.83	<u>18.62</u>	<u>18.62</u>	0	0.69	0
	Eddy Identification	204	3.93	0.49	3.92	4.9	<u>44.1</u>	1.47	4.9	14.22
	Marine Fog ..	200	<u>67.5</u>	55	61	<u>57</u>	53.5	3	55.5	<u>55.5</u>
	Marine Pollution...	110	0	0.91	2.73	2.73	<u>3.64</u>	0.91	2.73	<u>8.18</u>

A.6 Detailed results of specific sub-tasks (L-3 capability).

This section highlights the performance of MLLMs across all L-3 capabilities. The VQA task is split into perception, General reasoning, and Scientific-Knowledge Reasoning dimensions, with results shown in Tables 14. Model performance varies across L3 dimensions: InterVL3 excels in perception,

Table 14: **VQA Performance in L3 dimension.** We mark the highest score of each metric in red, and second highest underlined.

L4-task	Qwen2.5-VL		InternVL3		LLaVA-OV 7B	GPT-4o	Gemini	Claude3
	7B	72B	8B	78B				
Perception	13.42	15.37	<u>35.77</u>	24.68	34.66	15.40	33.33	26.97
General Reasoning	7.32	10.86	<u>28.67</u>	27.48	<u>30.71</u>	3.62	21.22	13.74
Scientific-Knowledge Reasoning	8.2	5.72	<u>30.89</u>	27.49	30.18	8.74	23.66	<u>31.62</u>

LLaVA-OneVision in general reasoning, and Claude3 in scientific knowledge reasoning. Overall, InterVL3 shows consistently strong results, while Qwen2.5VL and GPT-4o fall notably behind.

A.7 Samples and challenging Cases of OmniEarth-Bench

In this section, we construct a detailed table (Tab. 15) analyzing model performance and error causes for the L-4 subtask. We then use examples to thoroughly illustrate the errors for typical subtasks. In this section, we present a case study analysis of the error types made by Gemini-2.0-Flash [77], Qwen2.5-VL [5], and InterVL3 [104] on various sub-tasks in OmniEarth-Bench. We classify the errors into the following 6 categories:

Spatio-temporal Frame Confusion : The model misinterprets either the time sequence or the spatial orientation / coordinate frame of the data, leading to a reversed trend, direction, or geographic reference. See examples in Fig. 7, Fig. 13, etc.

Threshold / Severity Mis-estimation : Numeric values are read incorrectly or wrong thresholds are applied, so strength or severity categories are wrong. See examples in Fig. 12, Fig. 15, etc.

Image-feature Misinterpretation : Visual cues (texture, color, shape) are misread; key features are missed or artefacts are mistaken for real features. See examples in Fig. 16, Fig. 17, etc.

Domain-knowledge / Semantic Mis-match : Mis-application of non-visual expertise – ecology, climate thresholds, hazard mechanics – so the scene is matched to an incorrect knowledge template. See examples in Fig. 9.

Over-cautious / Refusal : Adequate information is available, but the model answers “Unable to decide” (or hedges) to avoid committing. See examples in Fig. 8, Fig. 10, etc.

Target Mis-location : The object or area specified in the prompt is not correctly identified, so all subsequent reasoning is off target. See examples in Fig. 14.

Table 15: Table index of case study figures by sub-tasks (L-3 capability) with associated (error) categories for each MLLM.

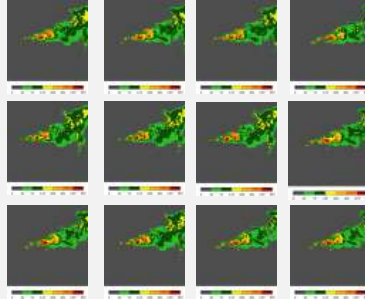
Case	L-1 task	L-4 task	Gemini	Qwen2-VL	InternVL3
Fig. 7	Atmosphere	Movement Prediction	Spatio-temporal Frame Confusion	Spatio-temporal Frame Confusion	Correct
Fig. 8	Biosphere	Dead Oil Palm counting	Correct	Over-cautious / Refusal	Over-cautious / Refusal
Fig. 9	Biosphere	Species Distribution Prediction	Correct	Domain-knowledge / Semantic Mis-match	Correct
Fig. 10	Cross-sphere	Most likely species to occur	Correct	Over-cautious / Refusal	Over-cautious / Refusal
Fig. 11	Cross-sphere	Global Flood Forecasting	Correct	Domain-knowledge / Semantic Mis-match	Image-feature Misinterpretation
Fig. 12	Cryosphere	SIC Estimate SIT	Correct	Image-feature Misinterpretation	Image-feature Misinterpretation
Fig. 13	Cryosphere	Sea Ice Extent Estimation	Spatio-temporal Frame Confusion	Threshold / Severity Mis-estimation	Over-cautious / Refusal
Fig. 14	Lithosphere	P-wave phase picking	Target Mis-location	Image-feature Misinterpretation	Threshold / Severity Mis-estimation
Fig. 15	Oceansphere	ENSO Identification	Domain-knowledge / Semantic Mis-match	Spatio-temporal Frame Confusion	Image-feature Misinterpretation
Fig. 16	Oceansphere	Marine Fog Detection	Threshold / Severity Mis-estimation	Image-feature Misinterpretation	Image-feature Misinterpretation
Fig. 17	Human-activity sphere	Fine-grained object type recognition	Image-feature Misinterpretation	Image-feature Misinterpretation	Image-feature Misinterpretation
Fig. 18	Lithosphere	earthquake source-receiver distance inference	Image-feature Misinterpretation	Image-feature Misinterpretation	Image-feature Misinterpretation
			Correct	Target Mis-location	Over-cautious / Refusal

Atmosphere

"Question": The provided image sequence represent the evolution of a convective system. What is the moving direction of the convective system in the sequence?

- (A) to west
- (B) to north
- (C) to south
- (D) to east
- (E) Unable to decide"

"Correct Answer": "D"



Spatio-temporal Frame Confusion

Gemini: "A"

"Reasoning": "The sequence of images shows the convective system moving from right to left. This indicates that the system is moving towards the west."



Spatio-temporal Frame Confusion

Qwen: A

"Reasoning": "The convective system is moving to the west. This is evident from the sequence of images where the red and yellow areas, indicating intense convective activity, are gradually shifting towards the left side of the frame. The green areas, representing less intense activity, are expanding towards the right, which further supports the westward movement. The overall pattern of the system's evolution shows a consistent westward progression over time."



Internvl3: D

"Reasoning": "The sequence of images shows the progression of a convective system over time. By observing the position and movement of the red and yellow areas, which represent higher temperatures or convective activity, we can see that the system is moving from the left side of the images to the right. This indicates a movement to the east."

Figure 7: A sample case of Movement Prediction subtask.

Biosphere

"Question": "This is an unmanned aerial vehicle (UAV) image capturing oil palm trees. How many dead trees are in this image?"

- (A) 3
- (B) 8
- (C) 11
- (D) 1
- (E) Unable to decide



"Correct Answer": "D"



Gemini: D

"Reasoning": "Based on the image, I can only identify one tree that appears to be dead or severely damaged. It is located in the upper-middle section of the image, and it has a significantly different color and structure compared to the healthy green oil palm trees."



Over-cautious / Refusal

Qwen:E

"Reasoning": "The image shows a dense plantation of oil palm trees with no clear signs of dead trees. The trees appear uniformly green and healthy, with no visible brown or withered foliage that would indicate dead trees. The image resolution and angle may not be sufficient to detect subtle signs of tree death. Without more detailed information or a closer view, it is not possible to accurately count dead trees. Therefore, the best answer is 'E' - Unable to decide."



Over-cautious / Refusal

Internvl3:E

"Reasoning": "The image shows a large number of oil palm trees, but it is difficult to determine the exact number of dead trees without a closer inspection or additional information. The trees appear healthy and green, but there are no clear indicators of dead trees visible from this aerial view."

Figure 8: A sample case of Dead Oil Palm counting subtask.

Biosphere

"Question": "Which species is most likely to live in the region shown at the image? The latitude is 60.1805513699° N, and the longitude is 24.9494441843° E."

- (A) *Fringilla coelebs gengleri*
- (B) *Acridotheres tristis*
- (C) *Passer domesticus*
- (D) *Anthornis melanura*
- (E) Unable to decide



"Correct Answer": "C"



Gemini: D

"Reasoning": "The coordinates 60.1805513699° N, 24.9494441843° E indicate Helsinki, Finland. The image shows an urban environment. *Passer domesticus* (House Sparrow) is a common bird species found in urban areas worldwide, including Europe. The other options are less likely: *Fringilla coelebs gengleri* is a subspecies of Chaffinch found in the British Isles, *Acridotheres tristis* (Indian Myna) is native to Asia, and *Anthornis melanura* (New Zealand Bellbird) is native to New Zealand."



Domain-knowledge / Semantic Mis-match

Qwen:E

"Reasoning": "The image shows a region with a mix of urban and green spaces, likely in a temperate climate zone. The coordinates place this region in Helsinki, Finland. *Fringilla coelebs gengleri*, a subspecies of the common chaffinch, is native to northern Europe and well-adapted to such environments. *Acridotheres tristis*, the common myna, is native to South Asia and not typically found in this region. *Passer domesticus*, the house sparrow, is common in urban areas but is not specific to this location. *Anthornis melanura melanura*, the tui, is native to New Zealand and not found in Europe. Therefore, *Fringilla coelebs gengleri* is the most likely species to live in this region."



Internvl3:E

"Reasoning": "The image shows a densely populated urban area with water bodies, which is characteristic of many cities in temperate regions. The latitude and longitude provided suggest a location in the northern hemisphere, likely in a region with a temperate climate. The species listed are birds, and among them, *Passer domesticus*, commonly known as the house sparrow, is known to inhabit urban environments. The other species listed are either not typically found in urban settings or are more specific to different regions. Therefore, *Passer domesticus* is the most likely species to live in the region shown in the image."

Figure 9: A sample case of Species Distribution Prediction subtask.

Cross-sphere

"Question": "This image shows the satellite view of a bird hotspot, which is located at longitude 34.356469 and latitude -0.738459 in the state of Nyanza, Kenya. ...Which of the following bird species is most likely to occur in this hotspot?"

- (A) *Pitta angolensis*
- (B) *Amadina fasciata*
- (C) *Streptopelia semitorquata*
- (D) *Spatula querquedula*
- (E) Unable to decide



"Correct Answer": "D"



Gemini: C

"Reasoning": "The image shows a landscape with a mix of vegetation and some built-up areas. The climate data indicates a relatively warm and wet environment. *Streptopelia semitorquata* (Red-eyed Dove) is a common bird in African woodlands and cultivated areas, which aligns with the habitat and climate suggested by the image and data. The other options are less likely: *Pitta angolensis* prefers dense forests, *Spatula querquedula* is a migratory duck and *Amadina fasciata* prefers drier areas."



Over-cautious / Refusal

Qwen: B

"Reasoning": "The satellite image shows a region with a mix of green vegetation and some human settlements, indicating a semi-arid to sub-humid environment. The bioclimatic variables suggest a warm climate with moderate precipitation, typical of savanna or woodland habitats. *Amadina fasciata*, commonly known as the black-rumped shama, is well-adapted to such environments. It prefers open woodlands and savannas, which align with the visual cues from the image. The other options are less likely: *Pitta angolensis* prefers dense forests, *Streptopelia semitorquata* is more common in arid regions, *Spatula querquedula* is a waterfowl requiring wetlands, and selecting 'E' would be too uncertain given the clear habitat match for *Amadina fasciata*."



Over-cautious / Refusal

Internvl3: A

"Reasoning": "The satellite image shows a bird hotspot in Nyanza, Kenya, with specific bioclimatic variables. *Pitta angolensis*, also known as the Angola Pitta, is known to inhabit areas with dense vegetation and a range of temperatures and precipitation levels similar to those described. The image shows a mix of agricultural fields and forested areas, which aligns with the habitat preferences of the Angola Pitta. The other options, such as *Amadina fasciata*, *Streptopelia semitorquata*, and *Spatula querquedula*, have different habitat requirements and are less likely to be found in this type of environment."

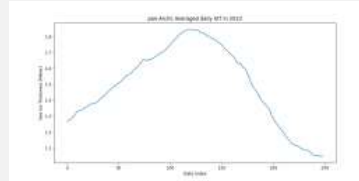
Figure 10: A sample case of Most likely species to occur subtask.

Cross-sphere

"Question": "As a pan-Arctic researcher, you are given one sea ice concentration map (the first image) and one plot for daily trend in sea ice thickness (the second image). Considering the date of SIC map is the following day of the end of SIT trend plot, which choice would most likely to be the averaged SIT of the given SIC map?"



- (A) 0.946
- (B) 1.775
- (C) 1.369
- (D) 1.052
- (E) Unable to decide"



"Correct Answer": "D"



Gemini: B

"Reasoning": "The SIC map is for the day after the SIT trend plot ends. The SIT trend plot ends at a date index of approximately 250, where the SIT is around 1.05 meters. Therefore, the most likely average SIT for the SIC map is 1.052."



Image-feature Misinterpretation

Qwen:C

"Reasoning": "The SIT plot shows a clear downward trend, ending at approximately 1.1 meters. The SIC map indicates a significant amount of sea ice coverage, suggesting that the SIT is not at its lowest point. Given the options, 1.369 meters is the most reasonable choice as it is higher than the endpoint of the SIT plot but lower than the peak, aligning with the expected SIT for the next day."



Image-feature Misinterpretation

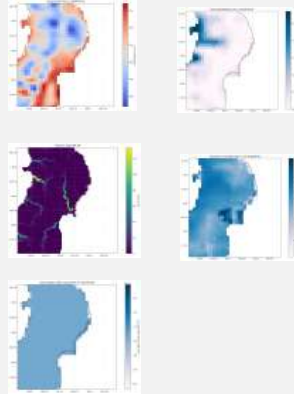
Internvl3:A

"Reasoning": "The SIT trend plot shows a decreasing trend in sea ice thickness over time. The date of the SIC map is the following day after the end of the SIT trend plot. By examining the plot, the SIT value at the end of the trend (around day 250) is approximately 1.1 meters. Given the decreasing trend, the SIT on the following day would likely be lower than 1.1 meters. Among the provided choices, 0.946 is the only value lower than 1.1 meters, making it the most likely averaged SIT for the given SIC map."

Figure 11: A sample case of Global Flood Forecasting subtask.

Cryosphere

"Question": "The first image is the GloFAS dis24 data, which represents the forecasted river discharge in cubic meters per second (m^3/s). The second image is the ERA5 temperature data at 2 meters above ground level, measured in Kelvin (K). The third image is the volumetric soil water content in the top layer of the soil, measured in cubic meters per cubic meter (m^3/m^3). The fourth image is the snow depth water equivalent, measured in meters (m). The fifth image is the total precipitation sum, measured in millimeters (mm). Whether flood occurs in the region on the date shown in the images ?"



- (A) Flooding occurs
- (B) Flooding does not occur
- (C) Unable to decide

"Correct Answer": "B"



Gemini: B

"Reasoning": "The river discharge (dis24) shows moderate levels in the rivers. The total precipitation sum is very low, indicating no significant rainfall. The soil water content is also not particularly high. The snow depth water equivalent is negligible. Therefore, based on the available data, flooding is unlikely to occur."



Threshold / Severity Mis-estimation

Qwen:C

"Reasoning": "The GloFAS dis24 data shows relatively low river discharge values, with no significant areas indicating high discharge that would typically suggest flooding. The temperature data does not show any extreme conditions that would contribute to flooding, such as rapid snowmelt. The soil water content is moderate, with no signs of saturation that could lead to runoff. The snow depth water equivalent is very low, indicating minimal snowmelt contribution. The total precipitation sum is also low, with no heavy rainfall that could cause flooding. However, without additional context or data, such as real-time river levels or local topography, it is not possible to definitively conclude whether flooding occurs or not."



Domain-knowledge / Semantic Mis-match

Internvl3:A

"Reasoning": "The first image shows high river discharge values, indicating potential flooding. The volumetric soil water content is high, suggesting saturated soil conditions. The snow depth water equivalent is also significant, which could contribute to runoff. The temperature is relatively low, which might slow down evaporation, further increasing the risk of flooding. These factors combined suggest that flooding is likely to occur in the region on the date shown."

Figure 12: A sample case of SIC Estimate SIT subtask.

Cryosphere

"Question": "As a geoscientist, you are given two sea ice concentration maps, which one describes the sea ice extent in Antarctic region?"

- (A) The first sea ice concentration map
- (B) The second sea ice concentration map
- (C) Both sea ice concentration maps
- (D) Neither
- (E) Unable to decide

"Correct Answer": "A"



Spatio-temporal Frame Confusion

Gemini: B

"Reasoning": "The second image shows a significantly reduced sea ice extent compared to the first image. During the melting season, sea ice extent decreases substantially due to warmer temperatures. Therefore, the second image is more likely to represent sea ice extent during the melting season."



Spatio-temporal Frame Confusion

Qwen: B

"Reasoning": "The second sea ice concentration map shows a significantly reduced area of sea ice compared to the first map. This is indicative of the melting season, where sea ice extent typically decreases. The first map displays a larger and more continuous ice coverage, suggesting it represents a time of year with less melting, such as winter or early spring. The second map's fragmented and reduced ice coverage aligns with the characteristics of the melting season, where ice retreats and breaks up. Therefore, the second map is more likely to represent the sea ice extent during the melting season."



Internvl3: A

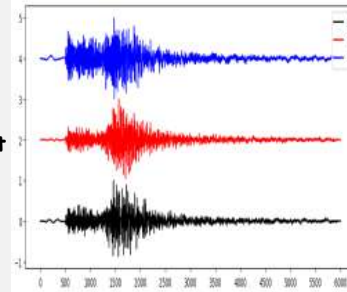
"Reasoning": "The first sea ice concentration map shows a large ice-covered area in the southern hemisphere, which is characteristic of the Antarctic region. The second map shows ice in the northern hemisphere, which is characteristic of the Arctic region. Therefore, the first map describes the sea ice extent in the Antarctic region."

Figure 13: A sample case of Sea Ice Extent Estimation subtask.

Lithosphere

"Question": "As a seismic waveform analyst, determine the exact onset of P-wave phases in three-component ENZ seismic data (East, North, Vertical; 0-6000 samples at 100Hz sampling rate). Prioritize vertical-component analysis validated by transverse energy analysis, with supplementary horizontal-component polarization verification. Output a integer [x] relative to sample index 0, rounded to nearest phase estimate."

- (A) 322
- (B) 500
- (C) 1317
- (D) 613
- (E) Unable to decide"



"Correct Answer": "B"



Target Mis-location + Domain-knowledge / Semantic Mis-match

Gemini: C

"Reasoning": "The P and S wave arrivals appear to be nearly simultaneous, occurring around sample 1400. With a sampling rate of 100 Hz, the P-S time difference is very small, suggesting a very short epicentral distance. Of the choices provided, 10 km is the only plausible distance for such a small time difference."



Target Mis-location + Domain-knowledge / Semantic Mis-match

Qwen: C

"Reasoning": "The image lacks clear P and S wave arrivals, making it impossible to determine the P-S time differential. Without this crucial information, calculating the epicentral distance is not feasible. The waveforms do not show distinct polarization characteristics that could aid in validation. The data appears noisy, further complicating analysis. Standard crustal velocity models cannot be applied effectively here. Therefore, an accurate estimate cannot be made."



Target Mis-location + Domain-knowledge / Semantic Mis-match

Internvl3: A

"Reasoning": "The waveform shows distinct P-wave arrivals in the East (E) and North (N) components, with a noticeable delay between them. The vertical (Z) component shows a clear P-wave arrival as well. By analyzing the time difference between the P-wave arrivals in the E and N components, we can estimate the epicentral distance. Assuming standard crustal velocities, the time difference corresponds to a distance of approximately 28 kilometers. This is consistent with the choices provided, making option (B) the best estimate."

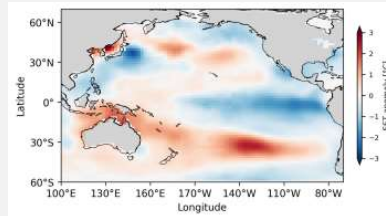
Figure 14: A sample case of P-wave phase picking subtask.

Oceansphere

"Question": "The following figure is a chart of Pacific Ocean sea surface temperature anomalies for DJF (December-January-February) season. Please judge the El Niño-Southern Oscillation (ENSO) event that occurred. If the Niño3.4 index is greater than 0.5 and less than 1.4, it is a weak/moderate El Niño; greater than 1.5 is a strong El Niño; greater than -1.4 and less than -0.5 is a weak/moderate La Niña; less than -1.5 is a strong La Niña."

- (A) Not an obvious event
- (B) Weak/Moderate El Niño
- (C) Strong El Niño
- (D) Weak/Moderate La Niña
- (E) Strong La Niña
- (F) Unable to decide

"Correct Answer": "D"



Threshold / Severity Mis-estimation

Gemini: E

"Reasoning": "The image shows sea surface temperature anomalies in the Pacific Ocean. There is a clear area of strong negative anomalies (blue color, indicating cooler than average temperatures) in the central and eastern equatorial Pacific. The color bar indicates that the anomalies are less than -1.5°C . This indicates a strong La Niña event."



Spatio-temporal Frame Confusion

Qwen: C

"Reasoning": "The image shows a significant warming in the central and eastern Pacific, particularly in the Niño3.4 region, which is a key indicator of El Niño. The color gradient indicates temperatures well above the 0.5°C threshold, suggesting a strong event. The Niño3.4 index appears to exceed 1.5°C , which classifies it as a strong El Niño. The widespread warming across the Pacific further supports this conclusion. No cooling patterns indicative of La Niña are present. Therefore, the event depicted is a strong El Niño."



Spatio-temporal Frame Confusion

Internvl3: B

"Reasoning": "The image shows sea surface temperature anomalies in the Pacific Ocean. The Niño3.4 region, typically located in the central Pacific, is indicated by the red and orange areas. These regions show warmer than average temperatures, suggesting an El Niño event. The anomalies are not extreme enough to classify as a strong El Niño, as they do not exceed 1.5°C . Therefore, the event is best described as a weak/moderate El Niño."

Figure 15: A sample case of ENSO Identification subtask.

Oceansphere

"Question": "The following image is an RGB image derived using the visible bands of satellite data. Please determine whether there is marine fog in the area shown in the image."

- (A) Yes, there is marine fog
- (B) No, there is no marine fog
- (C) Unable to decide

"Correct Answer": "B"



Image-feature Misinterpretation

Gemini: A

"Reasoning": "The image shows extensive areas of low-lying, featureless white or greyish features over the water. These features are consistent with marine fog or low stratus clouds. The texture and spatial distribution suggest a widespread phenomenon, likely fog."



Image-feature Misinterpretation

Qwen: A

"Reasoning": "The image shows a large body of water with a significant area covered by a uniform layer of white clouds, which is characteristic of marine fog. The fog appears to be hugging the coastline and extending over the water, a typical pattern for marine fog. The surrounding landmasses are visible with clear distinctions, indicating that the fog is localized over the water. The texture of the cloud layer is smooth and consistent, further suggesting the presence of marine fog. The absence of sharp cloud edges and the gradual transition from the fog to clearer areas support this conclusion."



Image-feature Misinterpretation

Internvl3:A

"Reasoning": "The image shows a satellite view with visible bands that highlight different features. The presence of marine fog can be inferred from the areas where the water appears lighter and more diffuse compared to the surrounding darker waters. This lighter appearance is characteristic of fog, which scatters light and reduces visibility. Additionally, the fog appears to be concentrated along the coastline, which is typical for marine fog formation."

Figure 16: A sample case of Marine Fog Detection subtask.

Human-activities sphere

"Question": "Recognize the category of objects from satellite and aerial images given the bounding boxes for referring objects. Bounding box in the format (xmin, ymin, xmax, ymax), where the top left corner is (x_min, y_min) and the bottom-right corner is (x_max, y_max). The resolution of satellite image is 600 x 600. Bounding box: [132, 142, 186, 187]"

- (A) flat_roof
- (B) gable_roof
- (C) row roof shed
- (D) Other
- (E) Unable to decide



"Correct Answer": "D"



Image-feature Misinterpretation

Gemini: A

"Reasoning": "The bounding box [132, 142, 186, 187] refers to a building with a flat roof. The roof appears to be uniformly flat without any visible gables or other roof structures."



Image-feature Misinterpretation

Qwen: A

"Reasoning": "The image shows a large industrial or commercial area with numerous buildings. The roofs of these buildings are predominantly flat, which is a common feature in industrial and commercial architecture. The flat roofs are visible as large, smooth surfaces with no significant slope or gable structures. The presence of parking lots and the layout of the buildings further suggest that these are likely warehouses or factories, which typically have flat roofs for practical reasons such as ease of construction and maintenance. Therefore, the category of objects in the bounding box is best described as 'flat_roof'."



Image-feature Misinterpretation

Internvl3: A

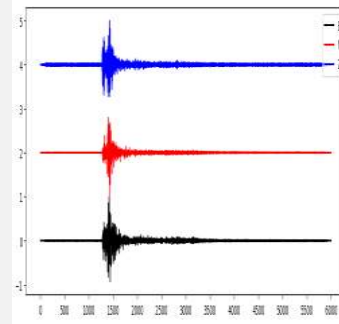
"Reasoning": "The bounding box coordinates provided correspond to a flat-roofed structure in the image. The area within the bounding box shows a rectangular shape with a flat surface, typical of flat roofs commonly found in industrial or commercial buildings. The lack of visible sloping edges or peaks further supports this classification."

Figure 17: A sample case of Fine-grained object type recognition subtask.

Lithosphere

"Question": "As a seismic waveform analyst, infer the epicentral distance (in kilometers) between the seismic receiver and earthquake source using three-component ENZ data (East, North, Vertical; 0-6000 samples at 100Hz sampling rate). Prioritize P-S arrival time differential analysis with polarization validation, assuming standard crustal velocity models. Output must be a single integer [x] representing the closest whole-kilometer estimate."

- (A) 10
- (B) 28
- (C) 50
- (b) -7
- (E) Unable to decide"



"Correct Answer": "A"



Gemini: A

"Reasoning": "The P and S wave arrivals appear to be nearly simultaneous, occurring around sample 1400. With a sampling rate of 100 Hz, the P-S time difference is very small, suggesting a very short epicentral distance. Of the choices provided, 10 km is the only plausible distance for such a small time difference."



Target Mis-location + Domain-knowledge / Semantic Mis-match

Qwen: E

"Reasoning": "The image lacks clear P and S wave arrivals, making it impossible to determine the P-S time differential. Without this crucial information, calculating the epicentral distance is not feasible. The waveforms do not show distinct polarization characteristics that could aid in validation. The data appears noisy, further complicating analysis. Standard crustal velocity models cannot be applied effectively here. Therefore, an accurate estimate cannot be made."



Target Mis-location + Domain-knowledge / Semantic Mis-match

Internvl3: B

"Reasoning": "The waveform shows distinct P-wave arrivals in the East (E) and North (N) components, with a noticeable delay between them. The vertical (Z) component shows a clear P-wave arrival as well. By analyzing the time difference between the P-wave arrivals in the E and N components, we can estimate the epicentral distance. Assuming standard crustal velocities, the time difference corresponds to a distance of approximately 28 kilometers. This is consistent with the choices provided, making option (B) the best estimate."

Figure 18: A sample case of earthquake source-receiver distance inference subtask.

A.8 Datasheets

In this section, we document essential details about the proposed datasets and benchmarks following the CVPR Dataset and Benchmark guidelines and the template provided by Gebru *et al.* [20].

A.8.1 Motivation

The questions in this section are primarily intended to encourage dataset creators to clearly articulate their reasons for creating the dataset and to promote transparency about funding interests. The latter may be particularly relevant for datasets created for research purposes.

1. “*For what purpose was the dataset created?*”

A: Existing benchmarks for Earth science multimodal learning exhibit critical limitations in systematic coverage of geosystem components and cross-sphere interactions, often constrained to isolated subsystems (only in human-activity sphere or atmosphere) with limited evaluation dimensions (≤ 16 tasks). To address these gaps, we introduce **OmniEarth-Bench**, the first comprehensive multimodal benchmark spanning all six Earth science spheres (atmosphere, lithosphere, Oceansphere, cryosphere, biosphere and human-activity sphere) and cross-spheres with one hundred expert-curated evaluation dimensions.

2. “*Who funded the creation of the dataset?*”

A: The dataset creation was funded by the affiliations of the authors involved in this work.

A.8.2 Composition

Most of the questions in this section are intended to provide dataset consumers with the information they need to make informed decisions about using the dataset for their chosen tasks. Some of the questions are designed to elicit information about compliance with the EU’s General Data Protection Regulation (GDPR) or comparable regulations in other jurisdictions. Questions that apply only to datasets that relate to people are grouped together at the end of the section. We recommend taking a broad interpretation of whether a dataset relates to people. For example, any dataset containing text that was written by people relates to people.

1. “*What do the instances that comprise our datasets represent (e.g., documents, photos, people, countries)?*”

A: Our Benchmark comprises not only publicly available open-source datasets but also a significant portion of data manually extracted by experts from satellite imagery and raw observational sources. For example, Vegetation Monitoring uses satellite imagery from MODIS and expert-curated data from the Global Land Surface Satellite (GLASS), including Leaf Area Index, Fractional Vegetation Cover, and Peak Vegetation Coverage Area. All datasets utilized in OmniEarth-Bench are publicly accessible and nonprofit.

2. “*How many instances are there in total (of each type, if appropriate)?*”

A: OmniEarth-Bench consists of seven spheres, with a total of 29,855 annotated data instances.

3. “*Does the dataset contain all possible instances or is it a sample (not necessarily random) of instances from a larger set?*”

A: The images in OmniEarth-Bench are sourced from existing [85], [78], [18], [31], [8], [44], [24], [4], [63], [82], [68], [47], [84], [59], [67], [99], [81], [37], [28], [57], [34], [36], [30], [89], [56], [12], [69], [94], [27], [74], [71] datasets, but all textual annotations were independently created by us.

4. “*Is there a label or target associated with each instance?*”

A: Yes, each instance has been annotated and quality-checked by specialized experts.

5. “*Is any information missing from individual instances?*”

A: No, each individual instance is complete.

6. “*Are relationships between individual instances made explicit (e.g., users’ movie ratings, social network links)?*”

A: Yes, the relationship between individual instances is explicit.

7. “Are there recommended data splits (e.g., training, development/validation, testing)?”
A: The dataset is designed to evaluate the performance of MLLMs across various Earth spheres, so we recommend using it in its entirety as a test set.
8. “Is the dataset self-contained, or does it link to or otherwise rely on external resources (e.g., websites, tweets, other datasets)?”
A: OmniEarth-Bench is self-contained and will be open-sourced on platforms like Hugging Face, integrated into evaluation tools such as LLMs-Eval [95, 40] for easy use.
9. “Does the dataset contain data that might be considered confidential (e.g., data that is protected by legal privilege or by doctor–patient confidentiality, data that includes the content of individuals’ non-public communications)?”
A: No, all data are clearly licensed.
10. “Does the dataset contain data that, if viewed directly, might be offensive, insulting, threatening, or might otherwise cause anxiety?”
A: No, OmniEarth-Bench does not contain any data with negative information.

A.8.3 Collection Process

In addition to the goals outlined in the previous section, the questions in this section are designed to elicit information that may help researchers and practitioners create alternative datasets with similar characteristics. Again, questions that apply only to datasets that relate to people are grouped together at the end of the section.

1. “How was the data associated with each instance acquired?”
A: The images in OmniEarth-Bench are sourced from existing [85], [78], [18], [31], [8], [44], [24], [4], [63], [82], [68], [47], [84], [59], [67], [99], [81], [37], [28], [57], [34], [36], [30], [89], [56], [12], [69], [94], [27], [74], [71] datasets, all textual annotations were independently created by experts.
2. “What mechanisms or procedures were used to collect the data (e.g., hardware apparatuses or sensors, manual human curation, software programs, software APIs)?”
A: Our Benchmark comprises not only publicly available open-source datasets but also a significant portion of data manually extracted by experts from satellite imagery and raw observational sources. For example, Vegetation Monitoring uses satellite imagery from MODIS and expert-curated data from the Global Land Surface Satellite (GLASS), including Leaf Area Index, Fractional Vegetation Cover and Peak Vegetation Coverage Area. Moreover, for the Eddy data in oceansphere, the chlorophyll (CHL) data used in this study were obtained by applying the OCI empirical algorithm to Level-2 data acquired by the Geostationary Ocean Color Imager I (GOCI) aboard the Oceanography and Meteorology Satellite (COMS). After careful selection and integration, we compiled a comprehensive dataset covering 33 different data sources across all Earth spheres. Tab.2 is a summary of the data sources used for each Earth sphere.
3. “If the dataset is a sample from a larger set, what was the sampling strategy (e.g., deterministic, probabilistic with specific sampling probabilities)?”
A: Please refer to the details listed in the main text Section 3.1.

A.8.4 Preprocessing, Cleaning, and Labeling

The questions in this section are intended to provide dataset consumers with the information they need to determine whether the “raw” data has been processed in ways that are compatible with their chosen tasks. For example, text that has been converted into a “bag-of-words” is not suitable for tasks involving word order.

1. “Was any preprocessing/cleaning/labeling of the data done (e.g., discretization or bucketing, tokenization, part-of-speech tagging, SIFT feature extraction, removal of instances, processing of missing values)?”
A: Yes. During image collection, we prioritized selecting valuable satellite images for annotation. For linguistic annotation, three Level-3 subtasks—Regional Land Use Classification, Regional Counting, and Regional Counting with Change Detection—were marked with

red circles. This method, mimicking human interaction, was essential for providing clear, fine-grained region-level analysis on ultra-high-resolution images.

2. “Was the ‘raw’ data saved in addition to the preprocessed/cleaned/labeled data (e.g., to support unanticipated future uses)?”

A: Yes, raw data is accessible.

3. “Is the software that was used to preprocess/clean/label the data available?”

A: Yes, the necessary software used to preprocess and clean the data is publicly available.

A.8.5 Uses

The questions in this section are intended to encourage dataset creators to reflect on tasks for which the dataset should and should not be used. By explicitly highlighting these tasks, dataset creators can help dataset consumers make informed decisions, thereby avoiding potential risks or harms.

1. “Has the dataset been used for any tasks already?”

A: No.

2. “Is there a repository that links to any or all papers or systems that use the dataset?”

A: Yes, we will provide such links in the GitHub and the Huggingface repository.

3. “What (other) tasks could the dataset be used for?”

A: OmniEarth-Bench is suitable for various tasks across other Earth spheres. It covers 103 subtasks spanning six major Earth spheres plus Cross-sphere, and is capable of handling various other tasks.

4. “Is there anything about the composition of the dataset or the way it was collected and preprocessed/cleaned/labeled that might impact future uses?”

A: No.

5. “Are there tasks for which the dataset should not be used?”

A: N/A.

A.8.6 Distribution

Dataset creators should provide answers to these questions prior to distributing the dataset either internally within the entity on behalf of which the dataset was created or externally to third parties.

1. “Will the dataset be distributed to third parties outside of the entity (e.g., company, institution, organization) on behalf of which the dataset was created?”

A: No. The datasets will be made publicly accessible to the research community.

2. “How will the dataset be distributed (e.g., tarball on website, API, GitHub)?”

A: We will provide OmniEarth-Bench in the GitHub and the Huggingface repository.

3. “When will the dataset be distributed?”

A: We will create a repository to release the data once the paper is officially published, ensuring compliance with the anonymity principle.

4. “Will the dataset be distributed under a copyright or other intellectual property (IP) license, and/or under applicable terms of use (ToU)?”

A: Yes, the dataset will be released under the Creative Commons Attribution-NonCommercial-ShareAlike 4.0 International License.

5. “Have any third parties imposed IP-based or other restrictions on the data associated with the instances?”

A: No.

6. “Do any export controls or other regulatory restrictions apply to the dataset or to individual instances?”

A: No.

A.8.7 Maintenance

As with the questions in the previous section, dataset creators should provide answers to these questions prior to distributing the dataset. The questions in this section are intended to encourage dataset creators to plan for dataset maintenance and communicate this plan to dataset consumers.

1. “*Who will be supporting/hosting/maintaining the dataset?*”
A: The authors of this work serve to support, host, and maintain the datasets.
2. “*How can the owner/curator/manager of the dataset be contacted (e.g., email address)?*”
A: The curators can be contacted via the email addresses listed on our paper or webpage.
3. “*Is there an erratum?*”
A: There is no explicit erratum; updates and known errors will be specified in future versions.
4. “*Will the dataset be updated (e.g., to correct labeling errors, add new instances, delete instances)?*”
A: Future updates (if any) will be posted on the dataset website.
5. “*Will older versions of the dataset continue to be supported/hosted/maintained?*”
A: Yes. This initial release will be updated in the future, with older versions replaced as new updates are posted.
6. “*If others want to extend/augment/build on/contribute to the dataset, is there a mechanism for them to do so?*”
A: Yes, we will provide detailed instructions for future extensions.

A.9 Limitation and Potential Societal Impact

In this section, we discuss the limitations and potential societal impact of this work.

A.9.1 Potential Limitations

While **OmniEarth-Bench** provides a comprehensive benchmark for evaluating the perception and reasoning capabilities of MLLMs, there are several limitations to consider:

- **Scope of Sensors:** Although our benchmark includes 29,855 annotations and 109 subtasks, it may not cover all possible real-world scenarios. There could be additional sensor data, like multispectral data that were not included in this study, potentially limiting the generalizability of our findings.
- **Model and Dataset Diversity:** In this paper, we extensively evaluated general-purpose MLLMs. As new models emerge, their evaluation results will be added to our open-source leaderboard. Additionally, OmniEarth-Bench will also be expanded in dataset size and task diversity.

A.9.2 Potential Negative Societal Impact

- **Safety Risks:** OmniEarth-Bench is designed to evaluate the performance of vision-language multimodal models in six spheres and cross-sphere scenarios. However, excessive reliance on evaluation datasets may lead to overconfidence in autonomous systems, such as multimodal large models. It is crucial to implement adequate safety measures and human supervision when deploying these MLLMs to ensure public safety.
- **Environmental Impact:** Training MLLMs on large datasets and evaluating them using OmniEarth-Bench requires a certain amount of computational resources. To facilitate future research, we will maintain a leaderboard of MLLMs, removing the need for repeated evaluations of existing models.

A.10 Usage of LLM

Writing Assistance LLMs were utilized as an auxiliary tool in the preparation and refinement of this manuscript. This involved tasks such as proofreading for grammatical consistency, improving sentence structure for better flow, and rephrasing complex technical descriptions to enhance clarity for

a broader audience. The authors conducted a thorough review and editing of all AI-suggested text to ensure the scientific accuracy and integrity of the final content. The authors retain full responsibility for all statements, claims, and conclusions presented in this work.

Code and Script Development During the development phase, LLMs were employed to accelerate the creation of various scripts. This included generating boilerplate code for data processing pipelines (e.g., remapping and cropping algorithms), developing utility functions for data handling, and assisting in debugging evaluation protocols. All code generated or modified with the assistance of LLMs was manually verified, tested, and optimized by the authors to ensure its correctness, efficiency, and adherence to the project's requirements.

Benchmark Content Generation and Evaluation Beyond supporting tasks, LLMs were integral to the methodology for generating and evaluating parts of the OmniEarth-Bench dataset itself.

- **Initial Caption Generation:** For the image captioning task, a state-of-the-art LLM was used to generate preliminary scientific captions by synthesizing information from multispectral satellite imagery and corresponding textual disaster reports.
- **Automated Evaluation:** In the open-ended question format, an LLM served a critical role as an automated judge to assess the semantic correctness of model-generated answers against the ground-truth answers.

It is essential to note that all content generated by LLMs for the benchmark (i.e., captions) underwent a meticulous review and validation process by domain experts to guarantee scientific accuracy and factual consistency.